

Response letter of hess-2020-19-Report #2

Dear Anonymous Referee #1,

Please find the responses to the comments.

Comments made by the reviewer were highly insightful. They allowed us to greatly improve the quality of the manuscript. We described the response to the comments.

Each comment made by the reviewers is written in *italic* font. We numbered each comment as (n.m) in which n is the reviewer number and m is the comment number. In the revised manuscript, changes are highlighted in yellow.

We trust that the revisions and responses are sufficient for our manuscript to be published in *Hydrology and Earth System Sciences*

Responses to the comments of Referee #1

First of all, I would like to thank the authors for having carefully addressed all my comments. I also appreciate their effort in proposing a real-world application based on the data of Ciullo et al. (2017). However, I still do have a few comments.

(2.1) - In my previous review, I asked to clarify how are the authors planning to estimate the accuracy of flood awareness observations. The authors replied that “several previous studies obtained the proxy of the social memory by interview data (Barendrecht et al. 2019) and the number of Google searches (Gonzales and Ajami 2017)”. However, it is still not clear to me how is the authors’ modeling framework going to assimilate such social observations and how are they going to assign an error to such observations. Maybe this is a limitation that should be included in the discussion of the results.

→ We fully agree with this comment. When the modelled state variables cannot be directly observed, it is not straightforward to assimilate observations into a model. Particle filter and any other state-of-the-art data assimilation methods are generally flexible to this case since the nonlinear map h in equation (9) can deal with the complex relationship between model states and observable variables. In numerical weather prediction, it is an active research area to consider how to design the nonlinear map h and how to assign the observation error especially when we assimilate satellite observations. Using these previous findings, we should consider how to assimilate the indirect observation of social awareness as future work. This point was indeed unclear in the original version of the paper. We have clarified this point in the revised version of the paper.

Lines 519-530: “The major limitation of this study is that we assume the modeled state variables can directly be observed although it is difficult to directly observe state variables of the socio-hydrologic models. For example, it is impossible to directly observe social awareness of flood risk in the flood risk model and several previous studies obtained the proxy of the social memory by interview data (Barendrecht et al. 2019) and the number of Google searches (Gonzales and Ajami 2017). When these indirect observations are assimilated into a model, the (non-linear) observation operator (see equation (9)), the assignment of the observation error, and assimilation methods should be carefully designed as previously discussed in the context of numerical weather prediction (e.g., Sawada et al. 2019; Okamoto et al. 2019; Minamide and Zhang 2017). Future work will focus on the methodological development to efficiently assimilate observations in the social domain with complicated structure of observation operators and errors.”

(2.2) - I think it would be really interesting to read more about the use of such assimilation framework to better understand the human-flood dynamics. Right now the discussion of the results is more focused

on the numerical tool, its performances, and observations availability (which is great). However, in my opinion, it would be also interesting to discuss more in detail how such a tool could help us in advancing our understanding of the complex feedback between the human and flood systems. What about using the proposed approach for predictions in socio-hydrological modeling?

→ We fully agree with this comment. We believe that socio-hydrologic data assimilation is useful to reconstruct the historical human-flood interactions which includes unobservable state variables. In the atmospheric science, atmospheric reanalysis has been intensively analyzed to understand complex feedback between many physical processes in the atmosphere, which cannot be done by simply analyzing observation data due to their sparsity. As we do with the atmospheric reanalysis, socio-hydrologic reanalysis works as a reliable and spatio-temporally homogeneous dataset and may be helpful to deepen our understanding of human and flood. In addition, as we do with the atmospheric reanalysis, we can use the socio-hydrologic reanalysis as the initial condition to predict the future of socio-hydrologic processes. It is impossible to obtain the complete set of state variables and parameters by observation due to its sparsity so that data assimilation contributes to generating good initial conditions and future projection. Although we have already mentioned the concept of “socio-hydrologic reanalysis” in the original paper, this point was indeed unclear. We have clarified this point in the revised version of the paper.

Lines 581-592: “In the atmospheric science, atmospheric reanalysis has been intensively analyzed to understand complex feedback in the atmosphere, which cannot be done by analyzing only observation data due to their sparsity. Socio-hydrologic reanalysis can work as a reliable and spatio-temporally homogeneous dataset and may be helpful to deepen our understanding of human and water. In addition, socio-hydrologic reanalysis can be used as initial condition to predict the future change of socio-hydrologic processes as atmospheric scientists predict the future weather/climate using atmospheric reanalysis. Since it is impossible to directly observe all state variables and parameters as initial condition, socio-hydrologic reanalysis is crucially important for accurate prediction. Socio-hydrologic data assimilation has a high potential to improve our understanding of the complex feedback between social and flood systems and predict their future.”

(2.3) - *In the title use either “assimilation” or “integration”, they are synonymous but they do mean different things.*

→ Data assimilation is the technical term which indicates approaches to sequentially estimate the state from observations and model based on their errors. In scientific papers, data assimilation includes the specific methods such as particle filter, ensemble Kalman filter, and 4-D variational methods. Therefore, we cannot say data “integration”. On the other hand, we believe that model-data integration

can be used as a broader concept that includes the methods to estimate and understand the phenomena using both model and data. Note that model-data “assimilation” has not been used in the literature. What we do in this paper is data assimilation so that it is appropriate to include data assimilation in the title. Since many scientists in socio-hydrology may not be so familiar to data assimilation, we believe that using model-data integration in the title is helpful to get the broader audiences for this paper. We do understand that they mean different things as the reviewer suggested. However, given the above, we would like to continue to use both “data assimilation” and “model-data integration” in the title. We have decided not to change this aspect of the paper.

(2.4) - How is it possible to get awareness higher than 1?

→ In the equation, there are no reasons why awareness should not be higher than 1. It is not a normalized variable nor a ratio so that it can be higher than 1 when its decay rate is small, and the community repeatedly experiences severe floods. Because we do not imply that M is a normalized variable in the original version of the paper, we believe that it is unnecessary to mention this point. We have decided not to change this aspect of the paper.

(2.5) - I invite the authors to improve the overall quality of the figures and include all the information in the legend of figures 12-15 (ensemble, mean ensemble, observations).

→ We have improved most figures with the appropriate legend.

1 **Socio-hydrologic data assimilation: Analyzing human-flood interactions by model-**
2 **data integration**

3

4 Yohei Sawada¹, Risa Hanazaki²

5 ¹ Institute of Engineering Innovation, School of Engineering, the University of Tokyo,
6 Tokyo, Japan

7 ² Institute of Industrial Science, the University of Tokyo, Tokyo, Japan

8

9

10 Corresponding author: Y. Sawada, Institute of Engineering Innovation, the University of
11 Tokyo, Tokyo, Japan, 2-11-6, Yayoi, Bunkyo-ku, Tokyo, Japan, yohei.sawada@sogo.t.u-
12 tokyo.ac.jp

13

14 **Abstract**

15 In socio-hydrology, human-water interactions are simulated by mathematical models.
16 Although the integration of these socio-hydrologic models and observation data is
17 necessary to improve the understanding of the human-water interactions, the
18 methodological development of the model-data integration in socio-hydrology is in its
19 infancy. Here we propose to apply sequential data assimilation, which has been widely
20 used in geoscience, to a socio-hydrological model. We developed particle filtering for a
21 widely adopted flood risk model and performed an idealized observation system
22 simulation experiment and a real-data experiment to demonstrate the potential of the
23 sequential data assimilation in socio-hydrology. In these experiments, the flood risk
24 model's parameters, the input forcing data, and empirical social data were assumed to be
25 somewhat imperfect. We tested if data assimilation can contribute to accurately
26 reconstructing the historical human-flood interactions by integrating these imperfect
27 models and imperfect and sparsely distributed data. Our results highlight that it is
28 important to sequentially constrain both state variables and parameters when the input
29 forcing is uncertain. Our proposed method can accurately estimate the model's unknown
30 parameters even if the true model parameter temporally varies. The small amount of
31 empirical data can significantly improve the simulation skill of the flood risk model.

32 Therefore, sequential data assimilation is useful to reconstruct historical socio-
33 hydrological processes by the synergistic effect of models and data.

34

35

36

37 **1. Introduction**

38 Socio-hydrology is an emerging research field in which two-way feedbacks between
39 social and water systems are investigated (Sivapalan et al. 2012, 2014). Understanding
40 complex socio-hydrologic phenomena contributes to solving water crises around the
41 world. Socio-hydrology has been recognized as an important scientific grand challenge
42 to meet United Nations' Sustainable Development Goals (Di Baldassarre et al. 2019).

43

44 The most popular approach in socio-hydrology is to develop dynamic models which
45 compute non-linear interactions between human and water. For instance, Di Baldassarre
46 et al. (2013) developed a simplified model, which described human-flood interactions, to
47 understand the levee effect in which high levees generate a false sense of security and
48 induce social vulnerabilities to severe floods (see also Viglione et al. 2014; Ciullo et al.
49 2017). Van Emmerik et al. (2014) developed a stylized model, which described two-way
50 feedbacks between environment and economic activities, to understand the historical
51 competition for water between agricultural development and environment health in
52 Australia (see also Roobavannan et al. 2017). Pande and Savenije (2016) modeled
53 economic activities of smallholder farmers to analyze the agrarian crisis in Marathwada,
54 India. While socio-hydrologic models described above assumed the existence of a single

55 lumped decision maker, Yu et al. (2017) incorporated a collective action into their model
56 and analyzed the dynamics of community-managed flood protection systems in coastal
57 Bangladesh. Please refer to Di Baldassarre et al. (2019) for the comprehensive review of
58 socio-hydrologic modeling.

59

60 In addition to these modeling approaches, both qualitative and quantitative data related to
61 socio-hydrologic processes are important to understand human-water interactions. For
62 instance, Mostert (2018) revealed historical changes in river management from water
63 resources development to protection and restoration by analyzing qualitative data. Dang
64 and Konar (2018) applied econometric methods to analyze quantitative data in both
65 human and water domains and quantified the causal relationship between trade openness
66 and water use. Kreibich et al. (2017) performed the detailed case study analysis on paired
67 floods, consecutive flood events which occurred in the same region with the second flood
68 causing significantly lower damage. They found that the reduction of vulnerability played
69 a key role for successful adaptation to the second floods.

70

71 Although it is expected that the integration of model and data contributes to accurately
72 understanding the socio-hydrologic processes (Mount et al. 2016), the methodological

73 development of the model-data integration in socio-hydrology is in its infancy. Generally,
74 mathematical models can provide spatiotemporally continuous state variables and
75 quantitative scenarios for future socio-hydrologic developments. In addition,
76 mathematical models can quantitatively provide possible scenarios unrealized in the real-
77 world, which gives the insight to targeted processes (e.g., Viglione et al. 2014). The major
78 limitation of socio-hydrological models is that they are often inaccurate due to the
79 uncertainty in their input forcing, parameters, and descriptions of the processes. On the
80 other hand, hydrologic and social data are often more reliable than numerical models and
81 can provide more complete understanding of the socio-hydrological processes (e.g.,
82 Mostert 2018), although data also have uncertainties. However, in many cases, relevant
83 data in socio-hydrology are sparsely distributed so that it is difficult to completely
84 reconstruct the historical socio-hydrologic processes from data. The other limitation of
85 the data-driven approach is that the quantification of the causal relationship cannot be
86 easily done only by empirical data (e.g., Dang and Konar 2018). Considering this
87 advantages and disadvantages of model and data, previous studies used social statistics
88 to calibrate and validate their socio-hydrologic models (e.g., Barendrecht et al. 2019;
89 Roobavannan et al. 2017; Ciullo et al. 2017; van Emmerik et al. 2014; Gonzales and
90 Ajami 2017).

91

92 In geosciences, sequential data assimilation has been widely used for the model-data
93 integration. Data assimilation sequentially adjusts the predicted state variables and
94 parameters of dynamic models by integrating observation data into models based on
95 Bayes' theorem. Data assimilation has been widely applied to numerical weather
96 prediction (e.g., Miyoshi and Yamane 2007; Bauer et al. 2015; Poterjoy et al. 2019;
97 Sawada et al. 2019), atmospheric reanalysis (e.g., Kobayashi et al. 2015; Hersbach et al.
98 2019), and hydrology and land surface modeling (e.g., Moradkhani et al. 2005; Sawada
99 et al. 2015; Rasmussen et al. 2015; Lievens et al. 2017). Applicability of the data
100 assimilation approach to the socio-hydrologic models has yet to be investigated.

101

102 In this study, we aim to develop the methodology of sequential data assimilation for the
103 flood risk model proposed by Di Baldassarre et al. (2013). From a series of idealized
104 experiments and a real-data experiment in the city of Rome, we demonstrate the potential
105 of data assimilation to accurately reconstruct the historical human-flood interactions. We
106 focus on the case in which the socio-hydrologic model's parameters, input forcing data,
107 and social data are somewhat inaccurate.

108

109

110 **2. Method**

111 **2.1. Model**

112 In this study, we used a socio-hydrologic flood risk model proposed by Di Baldassarre et
113 al. (2013). This model conceptualizes human-flood interactions by the set of simple
114 equations which describe the states of flood, economy, technology, politics, and society.
115 Based on this original model of Di Baldassarre et al. (2013), many similar flood risk
116 models have been proposed, validated, and applied (e.g., Viglione et al. 2014; Ciullo et
117 al. 2017; Barendrecht et al. 2019). Here we briefly describe this model. Please refer to Di
118 Baldassarre et al. (2013) for the complete description of this model.

119

120 The governing equations of the flood risk model are shown below:

$$121 \quad F = \begin{cases} 1 - \exp\left(-\frac{W + \xi_H H}{\alpha_H D}\right) & \text{if } W + \xi_H H > H \\ 0 & \text{if } W + \xi_H H \leq H \end{cases} \quad (1)$$

$$122 \quad R = \begin{cases} \varepsilon_T (W + \xi_H H - H) & \text{if } (F > 0) \text{ and } (FG > \gamma_E R \sqrt{G}) \text{ and } (G - FG > \gamma_E R \sqrt{G}) \\ 0 & \text{otherwise} \end{cases}$$

123 (2)

$$124 \quad S = \begin{cases} \alpha_S F & \text{if } (R > 0) \\ F & \text{if } (R = 0) \end{cases} \quad (3)$$

$$125 \quad \frac{dG}{dt} = \rho_E \left(1 - \frac{D}{\lambda_E}\right) G - \Delta(Y(t))(FG + \gamma_E R \sqrt{G}) \quad (4)$$

$$126 \quad \frac{dD}{dt} = \left(M - \frac{D}{\lambda_p}\right) \frac{\varphi_P}{\sqrt{G}} \quad (5)$$

$$127 \quad \frac{dH}{dt} = \Delta(Y(t))R - \kappa_T H \quad (6)$$

$$128 \quad \frac{dM}{dt} = \Delta(Y(t))S - \mu_S M \quad (7)$$

129

130 This model has four state variables: G , D , H , and M . $G(t)$ [L^2] is the size of the human
 131 settlement; $D(t)$ [L] is the distance of the center of mass of the human settlement from the
 132 river; $H(t)$ [L] is the flood protection level (or levee height); $M(t)$ [\cdot] is the social
 133 awareness of the flood risk. The timestep was set to annual.

134

135 Equation (1) calculates the intensity of flooding events $F(t)$ [\cdot] from the high water level
 136 $W(t)$ [L], the height of the levee $H(t)$ [L], and the distance of the human settlement from
 137 the river $D(t)$ [L]. Equation (2) calculates $R(t)$ [L], the amount by which the levees are
 138 raised responding to the flood event. There are three required conditions under which
 139 people decide to raise the levee. First, the flood event occurs. Second, the damage of flood
 140 (FG) should be larger than the cost of raising levee. Third, the cost of raising levee should
 141 be lower than the wealth remaining after the flooding. Equation (3) shows the magnitude
 142 of the psychological shock by the flood event $S(t)$ [\cdot]. If the levee is raised, the
 143 psychological shock is assumed to be mitigated. Equation (4) explains the dynamics of

144 $G(t)$, the size of the human settlement or the wealth of the community. Following the
145 notation of Di Baldassarre et al. (2013), $\Delta(Y(t)) = 1$ with integral only when time t
146 passes the time of the flooding event ($F > 0$), otherwise, $\Delta(Y(t)) = 0$. The term $FG +$
147 $\gamma_E R \sqrt{G}$ (total cost of flood damage and construction of levees) appears only if flood
148 occurs. Equation (5) shows the dynamics of the distance of the center of mass of the
149 human settlement from the river $D(t)$. When the social awareness of the flood risk is high,
150 people tend to live far from the river. Equation (6) computes the dynamics of the flood
151 protection level $H(t)$ and equation (7) shows the dynamics of the social awareness of the
152 flood risk $M(t)$. The explanation of parameters can be found in Table 1.

153

154

155 **2.2. Data Assimilation**

156 In this study, we used Sampling Importance Resampling Particle Filtering (SIRPF) as the
157 method of data assimilation. SIRPF has been widely used in hydrologic data assimilation
158 (e.g., Moradkhani et al. 2005; Qin et al. 2009; Sawada et al. 2015). Compared with the
159 other data assimilation algorithms such as ensemble Kalman filter, SIRPF is robust
160 against model nonlinearity and associated non-Gaussian error distribution. The
161 disadvantage of SIRPF is that the infeasible computational resources are required if the

162 numerical model is computationally expensive, which is not the case in the flood risk
163 model.

164

165 The flood risk model can be formulated as a discrete state-space dynamic system:

$$166 \quad \mathbf{x}(t + 1) = f(\mathbf{x}(t), \boldsymbol{\theta}, \mathbf{u}(t)) + \mathbf{q}(t) \quad (8)$$

167 where $\mathbf{x}(t)$ is the state variables (i.e. G, D, H, and M), $\boldsymbol{\theta}$ is the model parameters, $\mathbf{u}(t)$
168 is the external forcing (i.e., the high water level), and $\mathbf{q}(t)$ is the noise process which
169 represents the model error. In data assimilation, it is useful to formulate an observation
170 process as follows:

$$171 \quad \mathbf{y}^f(t) = h(\mathbf{x}(t)) + \mathbf{r}(t) \quad (9)$$

172 where $\mathbf{y}^f(t)$ is the simulated observation, h is the observation operator which maps the
173 model's state variables into the observable variables, and $\mathbf{r}(t)$ is the noise process which
174 represents the observation error.

175

176 The SIRPF is a Monte Carlo approximation of Bayesian update of the state variables and
177 parameters:

$$178 \quad p(\mathbf{x}(t), \boldsymbol{\theta} | \mathbf{y}^o(1:t)) \propto p(\mathbf{y}^o(t) | \mathbf{x}(t), \boldsymbol{\theta}) p(\mathbf{x}(t), \boldsymbol{\theta} | \mathbf{y}^o(1:t-1)) \quad (10)$$

179 where $p(\mathbf{x}(t), \boldsymbol{\theta} | \mathbf{y}^o(1:t))$ is the posterior probability of the state variables $\mathbf{x}(t)$ and
180 parameters $\boldsymbol{\theta}$ given all observations up to time t $\mathbf{y}^o(1:t)$. The prior knowledge,
181 $p(\mathbf{x}(t), \boldsymbol{\theta} | \mathbf{y}^o(1:t-1))$, based on the model integration is updated using the likelihood
182 which includes the new observation at time t $p(\mathbf{y}^o(t) | \mathbf{x}(t), \boldsymbol{\theta})$. In this study, we assumed
183 that our observation error follows Gaussian distribution so that the likelihood can be
184 formulated as follows:

$$185 \quad p(\mathbf{y}^o(t) | \mathbf{x}(t), \boldsymbol{\theta}) \equiv L(\mathbf{y}^o(t), \mathbf{x}(t), \boldsymbol{\theta}) =$$

$$186 \quad \frac{1}{\sqrt{\det(2\pi\mathbf{R})}} \exp \left[-\frac{1}{2} \left(\mathbf{y}^o(t) - \mathbf{y}^f(t) \right)^T \mathbf{R}^{-1} \left(\mathbf{y}^o(t) - \mathbf{y}^f(t) \right) \right] \quad (11)$$

187 where \mathbf{R} is the covariance matrix of the observation error process $\mathbf{r}(t)$. The prior
188 knowledge of the state variables is approximated by the ensemble simulation:

$$189 \quad p(\mathbf{x}(t) | \mathbf{y}^o(1:t-1)) \approx \frac{1}{N} \sum_{i=1}^N \delta \left[\mathbf{x}(t) - f \left(\mathbf{x}^i(t-1), \boldsymbol{\theta}^i, \mathbf{u}^i(t-1) \right) \right] \quad (12)$$

190 where N is the ensemble size, $\mathbf{x}^i, \boldsymbol{\theta}^i, \mathbf{u}^i$ are the realizations of the ensemble member i ,
191 and $\delta[\cdot]$ is the Dirac delta function.

192

193 The posterior probability of the state variables and parameters can be approximated as
194 follows:

$$195 \quad p(\mathbf{x}(t) | \mathbf{y}^o(1:t)) \approx \sum_{i=1}^N w(i) \delta(\mathbf{x}(t) - \mathbf{x}^i(t)) \quad (13)$$

$$196 \quad p(\boldsymbol{\theta} | \mathbf{y}^o(1:t)) \approx \sum_{i=1}^N w(i) \delta(\boldsymbol{\theta} - \boldsymbol{\theta}^i) \quad (14)$$

197 where $w(i)$ is the normalized weight for the realization of the ensemble member i and
198 is calculated using the likelihood (see also equation (11)).

$$199 \quad w(i) = \frac{L(\mathbf{y}^o(t), \mathbf{x}^i(t), \theta^i)}{\sum_{k=1}^N L(\mathbf{y}^o(t), \mathbf{x}^k(t), \theta^k)} \quad (15)$$

200 Note that equations (13) and (14) update all state variables and parameters of the model
201 although the weight is calculated using only observable variables. Therefore, it is not
202 necessary to observe all state variables in order to update all system variables.

203

204 The implementation of SIRPF is the following:

- 205 1. Model state variables are updated from time $t-1$ to t using ensemble
206 simulation (equations (8) and (12)).
- 207 2. Simulated observations are calculated for all ensembles (equation (9)).
- 208 3. The likelihood for each ensemble member is calculated (equation (11))
- 209 4. The weights are obtained for all ensembles (equation (15))
- 210 5. We applied a resampling procedure according to the normalized weights.

211 The normalized weights of ensemble i , $w(i)$, can be recognized as the
212 probability that the ensemble i is selected after resampling. Resampled state
213 variables and parameters are defined as \mathbf{x}_{resamp}^i and θ_{resamp}^i , respectively.

214 6. Since there are no mechanisms to increase the variance of parameters of
 215 ensemble members, Moradkhani et al. (2005) proposed to perturb the
 216 ensembles of parameters:

$$217 \quad \boldsymbol{\theta}^i \leftarrow \boldsymbol{\theta}_{resamp}^i + \varepsilon^i \quad (16)$$

$$218 \quad \varepsilon^i \sim N(0, \max(\boldsymbol{\omega}, s \times Var^\theta)) \quad (17)$$

219 where $N(\cdot)$ is the Gaussian distribution, Var^θ is the variance of $\boldsymbol{\theta}^i$, $\boldsymbol{\omega}$
 220 is the fixed hyperparameter (see Table 1 for its variable) which guarantees
 221 that the ensembles of parameters do not converge into a single value. s is
 222 an adaptively changed factor according to the effective ensemble size, N_{eff} .

$$223 \quad s = s_0 \left(1 - \left(\frac{N_{eff}}{N}\right)^2\right) \quad (18)$$

$$224 \quad N_{eff} = \frac{1}{\sum_{i=1}^N w(i)} \quad (19)$$

225 where $s_0 = 0.05$. The effective ensemble size is the measure of the
 226 diversity of ensembles. If the effective ensemble size becomes small,
 227 ensembles should be strongly perturbed in order to maintain the diversity of
 228 ensembles. Similar strategy has been used in many SIRPF systems (e.g.,
 229 Moradkhani et al. 2005; Poterjoy et al. 2019).

230

231

232 3. Experiment design

233 3.1. Observation System Simulation Experiment

234 In this study, we performed three observation system simulation experiments (OSSEs).

235 In the OSSE, we generated the synthetic truth of the state and flux variables by driving

236 the flood risk model with the specified parameters and input. Then, we generated

237 synthetic observations by adding the noise to this synthetic truth. Those synthetic

238 observations were assimilated into the model by SIRPF. The performance of SIRPF was

239 evaluated by comparing the estimated state variables by SIRPF with the synthetic truth.

240 Model parameters used to generate the synthetic truth can be found in Table 1. They are

241 identical to Di Baldassarre et al. (2013). The OSSE has been recognized as an important

242 preliminary step to verify the newly developed data assimilation systems (e.g.,

243 Moradkhani et al. 2005; Vrugt et al. 2013; Penny and Miyoshi 2016; Sawada et al. 2018).

244

245 The high water level for the synthetic truth was generated by the following:

$$246 \quad W = \min (v - 10, 0) \quad (20)$$

247 v follows the Gumbel distribution:

$$248 \quad p(v) = \frac{\exp(-\frac{v-\mu}{\beta})}{\beta} \exp(-\exp(-(v-\mu)\beta)) \quad (21)$$

249 where $\mu = 9, \beta = 2.5$. Although our high water level is not identical to Di Baldassarre
250 et al. (2013), the estimated trajectory of the state variables is similar to Di Baldassarre et
251 al. (2013).

252

253 Synthetic observations were generated by adding the Gaussian white noise to the F, G, D,
254 H, and M (see section 2.1) of the synthetic truth. The mean of the Gaussian white noise
255 was 0. The observation error, the standard deviation of the Gaussian white noise, was
256 firstly set to 10% of the synthetic true variables. Although this observation error is
257 generally larger than that used in meteorology and hydrology, we further increased the
258 observation error and tested the sensitivity of the observation error to the SIRPF's
259 performance. We firstly assumed that all of the F, G, D, H, and M can be observed every
260 10 years or every 10 model integration steps. Then, we evaluated the sensitivity of the
261 observation network (i.e. the observable variables and the observation intervals) to the
262 SIRPF's performance. Although it is not straightforward to observe social memory M,
263 several previous studies obtained the proxy of the social memory by interview data
264 (Barendrecht et al. 2019) and the number of Google searches (Gonzales and Ajami 2017).

265

266 We used the ensemble mean of root-mean square errors (mRMSE) as an evaluation
267 metrics:

$$268 \quad RMSE^i = \sqrt{\frac{1}{T} \sum_{t=1}^T (x^i(t) - z(t))^2} \quad (22)$$

$$269 \quad mRMSE = \frac{1}{N} \sum_{i=1}^N RMSE^i \quad (23)$$

270 where $RMSE^i$ is root-mean-square-error for i th ensemble, T is the computational period,
271 $x^i(t)$ is the simulated state variables of ensemble i at time t , $z(t)$ is the synthetic truth
272 at time t .

273

274

275 **3.1.1. Experiment 1: Perfect model with uncertain high water levels**

276 In the first OSSE, we assumed that there is no uncertainty in model parameters. We used
277 the same parameter variables as the synthetic truth run and we did not perform the
278 estimation of parameters. Our SIRPF updated only state variables. Although the model
279 had no uncertainty, it was assumed that the input data, the timeseries of the high water
280 level, were uncertain. Lognormal multiplicative noise was added to the synthetic true high
281 water level so that different ensemble members have different high water levels in the
282 data assimilation experiment. The two parameters of the lognormal distribution,
283 commonly called μ and σ , were set to 0 and 0.15, respectively.

284

285

286 **3.1.2. Experiment 2: Unknown model parameters and uncertain high water levels**

287 In the second OSSE, we assumed that some of the synthetic true parameter values were
288 unknown. The unknown parameters in the experiment 2 were the cost of levee raising γ_E ,
289 the rate by which new properties can be built φ_P , the rate of decay of levees κ_T , and
290 memory loss rate μ_S (see Table 1). We selected these unknown parameters one by one
291 from four equations of economy, politics, technology, and social to discuss how each state
292 variable's observation affects the estimation of parameters across these four equations
293 (see section 2.1). We have no unknown parameters related to F (equation (1)) since it is
294 unlikely that the parameters in equation (1) are much more inaccurate than the other
295 parameters. The parameters related to flood are mainly determined by the topography of
296 the flood plain so that the process described in equation (1) can be replaced by more
297 accurate hydrodynamic models in the real-world case study. The initial parameter
298 variables were assumed to be distributed in the bounded uniform distributions whose
299 ranges were found in Table 1. The uncertainty of the simulation induced by these
300 parameters' uncertainty is large enough to demonstrate the potential of data assimilation
301 to minimize the simulation's uncertainty (see Results). Our SIRPF sequentially

302 assimilated observations and estimated both state variables and parameters in the
 303 experiment 2. The high water level data were uncertain as the experiment 1.

304

305

306 **3.1.3. Experiment 3: Unknown and time-variant model parameters and uncertain**
 307 **high water levels**

308 To further demonstrate the potential of sequential data assimilation in socio-hydrology,
 309 we assumed that the description of the model was biased in the experiment 3. Here we
 310 assumed that two of the model parameters were temporally varied by the unknown
 311 dynamics. Specifically, the rate by which new properties can be built, φ_P , and the
 312 memory loss rate, μ_S , were temporally varied in the experiment 3:

$$313 \quad \varphi_P(t) = \begin{cases} 5000 & (t < 250) \\ 5000 + (t - 250) \times \frac{40000 - 5000}{500} & (250 \leq t < 750) \\ 40000 & (750 \leq t) \end{cases} \quad (24)$$

$$314 \quad \mu_S(t) = \begin{cases} 0.01 & (t < 250) \\ 0.01 + (t - 250) \times \frac{0.10 - 0.01}{500} & (250 \leq t < 750) \\ 0.10 & (750 \leq t) \end{cases} \quad (25)$$

315 In the data assimilation experiment, we assumed that the dynamics of φ_P and μ_S was
 316 unknown, and we integrated the flood risk model with time-invariant φ_P and μ_S . We
 317 evaluated if SIRPF could track this time-variant parameter and reveal the bias of the
 318 model's description. The cost of levee raising γ_E , and the rate of decay of levees κ_T

319 were assumed to be time-invariant unknown parameters as they were in the experiment
320 2. The cost of levee raising γ_E affects the state variables of the flood risk model mainly
321 in the initial early years and the gradual change of the rate of decay of levees κ_T has few
322 impacts on the state variables. Therefore, we found that it is difficult to track the temporal
323 change of these two parameters. The input forcing data, high water level, were uncertain
324 as described in the experiment 1.

325

326

327 **3.2. Real-data experiment**

328 In addition to the OSSEs, we performed the real-world experiment in the city of Rome,
329 Italy. Ciullo et al. (2017) collected real-world data and calibrated their flood risk model.
330 Using the data collected by Ciullo et al. (2017), we performed the data assimilation
331 experiment. It should be noted that the flood risk model of Ciullo et al. (2017) is different
332 from our model (i.e. Di Baldassarre et al. 2013), although they are conceptually similar.

333

334 All the data were collected from Figure 1 of Ciullo et al. (2017) by WebPlotDigitizer
335 (<https://automeris.io/WebPlotDigitizer/>). The observed high water level of Tiber River
336 was used as input forcing data (W). The levee height (H) and population (G) were used

337 as the observation data to be assimilated into the flood risk model. In Ciullo et al. (2017),
338 population values within the Tiber's floodplain were normalized by the theoretical
339 maximum Tiber's floodplain population which is estimated to the range between 10^6
340 and 2×10^6 . Since our flood risk model needs the population values (not normalized
341 values), we multiplied 1.5×10^6 and the normalized values shown in Figure 1 of Ciullo
342 et al. (2017) to obtain population in the floodplain.

343

344 We added lognormal multiplicative noise to the observed high water level as we did in
345 the OSSEs. The observation errors of levee height and population were set to 10% and
346 25% of the observed values, respectively. Since Ciullo et al. (2017) showed the large
347 uncertainty in the estimation of the theoretical maximum population (see above), it is
348 reasonable to assume that the estimation of population values also has relatively large
349 uncertainty.

350

351 As the second and third OSSEs, we have 4 unknown parameters in this real-world
352 experiment. We used the same settings of parameters as the OSSEs, which are shown in
353 Table 1, except for ξ_H , proportion of additional high water level due to levee heightening.
354 In this real-world experiment, we set $\xi_H = 0$ because the observed high water level

355 includes the effects of levee heightening. This treatment is consistent to Ciullo et al.
356 (2017) (see their Table 2).

357

358 The initial conditions of H and M were set to 0. The initial conditions of D were obtained
359 from the uniform distribution between 1000 and 5000. The initial conditions of G were
360 obtained from the uniform distribution between 1500 and 50000.

361

362

363 **4. Results**

364 **4.1. Observation System Simulation Experiment**

365 **4.1.1. Experiment 1: Perfect model with uncertain high water levels**

366 Figure 1 shows the timeseries of the model variables calculated by 5000 ensembles with
367 no data assimilation. Although the ensemble mean of the state variables is close to the
368 synthetic truth, the ensembles have the large spread especially for G. The uncertainty in
369 the input forcing brings the uncertainty in the estimation of the historical socio-hydrologic
370 condition.

371

372 Figure 2 indicates that this uncertainty is mitigated by assimilating the observations of F,
373 G, D, H, and M into the model every 10 years with 5000 ensembles. Table 2 shows that
374 RMSE is reduced for all state variables by data assimilation.

375

376 While we can observe all of F, G, D, H, and M in Figure 2 and Table 2, Figure 3 shows
377 the performance of our SIRPF in which only one of them can be observed. Our SIRPF
378 updates all state variables although only one of them is assimilated. Figure 3 reveals that
379 we can accurately propagate the observation information into the model state space. In
380 other words, our SIRPF can positively impact the estimation of not only observed state
381 variables but unobserved state variables. For instance, even if we can observe only G, the
382 simulation of all G, D, H, and M is improved. This finding is promising since all of the
383 state variables cannot be observed in the real-world applications. Figure 3 also shows that
384 observing F is not effective compared with the other variables. This is because F is a flux
385 and F can be observed only when floods occur so that the number of effective
386 observations is small. In addition, observing F, D, and M negatively impacts the
387 estimation of H and observing H does not significantly improve the simulation of D and
388 M. Although the dynamics of F, D, and M strongly affects the decision making of whether
389 the levees are raised or not, the amount by which the levees are raised, R, is fully

390 determined by the high water level, W , once the community determines to raise the levees
391 (see equation (2)). Therefore, the uncertainty of H is largely induced by the uncertainty
392 of the high water level, W , whose uncertainty is not directly mitigated by our SIRPF. This
393 is why observing F , D , and M is not helpful to mitigate the uncertainty of H .

394

395 While we can observe every 10 years in Figure 2 and Table 2, Figure 4 shows the
396 sensitivity of the observation intervals to the performance of our SIRPF. Our SIRPF
397 improves the estimation of the state variables when we can obtain observation once in
398 50-year or 100-year (see also Figure S1 for timeseries of the model's variables), which is
399 promising since we cannot expect the frequent observations in the real-world applications.

400

401 We set the observation error to 10% of the synthetic truth thus far. The improvement of
402 the simulation skill can be found with larger observation errors (Figure S2). Although the
403 SIRPF's performance gradually declines as the observation error increases, our SIRPF
404 can significantly improve the simulation skill with 25% observation error.

405

406 Although we demonstrate the potential of our SIRPF with 5000 ensembles thus far, the
407 improvement of the simulation skill can be found in much smaller ensemble sizes. The

408 performance of our SIRPF with 20 ensembles is similar to that with 5000 ensembles
409 (Figure S3).

410

411

412 **4.1.2. Experiment 2: Unknown model parameters and uncertain high water levels**

413 Figure 5 reveals that the flood risk model completely loses its skill to estimate the human-
414 flood interactions if there are uncertainties in model parameters and high water levels
415 prescribed in Section 3. In contrast to the experiment 1, the ensemble mean cannot
416 accurately reproduce the synthetic truth.

417

418 Figure 6 indicates that our SIRPF can accurately estimate the model state variables by
419 assimilating the observations of F, G, D, H, and M into the model every 10 years with
420 5000 ensembles. Figure 7 indicates that four unknown parameters can also be accurately
421 estimated. We find that it is relatively difficult to estimate the rate of levee's decay, κ_T ,
422 compared with the other parameters. This is because κ_T strongly affects the dynamics
423 of H and the uncertainty in H is largely determined by the uncertainty in high water levels,
424 which is not directly mitigated by our SIRPF system. Table 3 shows that RMSE is reduced
425 for both state variables and parameters by data assimilation.

426

427 We analyzed the impacts of the individual observation types on the simulation skill as we
428 did in the experiment 1. Figure 8a shows that the effects of the individual observation
429 types are similar to what we found in the experiment 1: (1) our SIRPF can improve the
430 skill to simulate unobservable state variables; (2) observing F is not effective compared
431 with the other observations; (3) observing H does not significantly improve the simulation
432 of D and M. Figure 8b reveals that the parameters can be efficiently estimated by
433 assimilating the observation of the state variables which are tightly related to the targeted
434 parameters. For instance, observing D can greatly improve the rate by which new
435 properties can be built, φ_P , in equation (5) which governs the dynamics of D. However,
436 assimilating a single observation type can contribute to accurately estimating all four
437 parameters in many cases, which is the promising result considering the sparsity of the
438 observation in the real-world applications.

439

440 The good performance of our SIRPF can be found with the longer observation intervals
441 as we found in the experiment 1. Figure 9 indicates that our SIRPF can improve the
442 estimation of the state variables and parameters when we can obtain observation once in
443 50-year or 100-year (see also Figures S4 and S5 for timeseries of the model's variables).

444

445 As we found in the experiment 1, the SIRPF's performance declines with the increased
446 observation error (Figure S6). However, it is promising that our SIRPF can improve the
447 simulation skill with larger observation errors up to 25% of the synthetic truth considering
448 that the observations in the socio-hydrologic domain are often inaccurate.

449

450 In contrast to the experiment 1, the larger ensemble size is required to stably estimate both
451 state variables and parameters (Figure S7). The increased degree of freedom and the
452 nonlinear relationship between parameters and observations increase the necessary
453 ensemble size.

454

455

456 **4.1.3. Experiment 3: Unknown and time-variant model parameters and uncertain**
457 **high water levels**

458 In addition to the experiment 2, two of the unknown parameters (φ_P and μ_S) temporally
459 vary in the synthetic truth of the experiment 3. We found that a larger spread of φ_P is
460 required to stably track the time-variant synthetic true φ_P so that we increased s_0 in
461 equation (18) from 0.05 to 0.5 only for φ_P in this experiment 3. Figure 10 and Table 4

462 indicate that despite the error in the model's description, our SIRPF can greatly improve
463 the simulation of the flood risk model. Please note that the synthetic truth shown in Figure
464 10 is different from that of the previous experiments especially for D and M. Figures 11b
465 and 11d indicate that we can accurately estimate the time-variant parameters (φ_P and
466 μ_S) as well as the other time-invariant parameters (Figures 11a and 11c). This result is
467 promising since we cannot expect the perfect description of the socio-hydrologic model
468 in the real-world applications. We also performed the sensitivity test on observation types,
469 observation intervals, and ensemble sizes, which results in the same conclusions as the
470 experiment 2 (not shown).

471

472

473 **4.2. Real-data experiment**

474 Figure 12 shows the timeseries of the model variables calculated by 5000 ensembles with
475 no data assimilation. The 5000-ensemble simulation reveals the two bifurcated social
476 systems. One builds a high levee and maintains a course of stable economic growth. The
477 other one has no levee and its economy is damaged by severe floods many times
478 (ensemble mean shown in Figure 12b implies that there are many ensemble members with
479 zero levee height).

480

481 In reality, the city of Rome constructed the levee responding to the severe flood occurred
482 on 28 December 1870. After the construction of this levee, no major flood losses occurred,
483 allowing the steady and undisturbed growth. Figure 13 indicates that our SIRPF
484 successfully constrains the trajectory of the ensemble simulation to the real-world (i.e.
485 high levee and stable economic growth) by assimilating the real data of H and G. Figure
486 S8 shows the SIRPF-estimated unknown parameters. Our SIRPF suggests lower γ_E than
487 the initial ensemble mean to promote the levee construction with lower costs. Lower κ_T
488 is also obtained because the assimilated real data show no decay of levee from 1874 to
489 2009. Compared with the OSSE experiment 2, the large uncertainty in estimated
490 parameters remains at the final timestep due to the limited number of assimilated
491 observations. In contrast to the OSSEs, our observation network has the uneven temporal
492 distribution. Figure 13 clearly indicates that our SIRPF is robust to these intermittent
493 observations whose intervals temporally change.

494

495 We analyzed the impacts of the individual observation types (i.e. H and G) on the
496 simulation skill as we did in the OSSEs. Figure 14 indicates that our SIRPF realistically
497 simulates the socio-hydrologic dynamics in the city of Rome and provides the similar

498 estimated state variables shown in Figure 13 by assimilating only population data. As we
499 found in the OSSEs, observations of the size of the human settlement G are informative
500 to effectively constrain the flood risk model. The dynamics of the parameter estimation
501 is similar to the case in which data of both G and H are assimilated (Figure S9).

502

503 On the other hand, assimilating only levee height data cannot provide the similar results
504 to those shown above. Figure 15 shows the timeseries of the model variables by the data
505 assimilation experiment in which we assimilated the observation data of H only.
506 Observations of the levee height cannot effectively constrain D , G , and M compared with
507 the observations of G . This finding is consistent to the OSSEs. The uncertainty in
508 estimated parameters becomes larger when we omit to assimilate observations of G
509 (Figure S10). Although the impact of levee height data is limited compared with
510 population data, it is promising that we can estimate the socio-hydrologic dynamics to
511 some extent only from the levee height data whose distribution is temporally sparse.

512

513

514 **5. Discussion**

515 In this study, we developed the sequential data assimilation system for the widely adopted
516 socio-hydrological model, the flood risk model by Di Baldassarre et al. (2013). We
517 demonstrated that our SIRPF for the flood risk model is useful to reconstruct the historical
518 human-flood interactions, which can be called “socio-hydrologic reanalysis”, by
519 integrating sparsely distributed observations and imperfect numerical simulation. In the
520 atmospheric science, atmospheric reanalysis has been intensively analyzed to understand
521 complex feedback in the atmosphere, which cannot be done by analyzing only
522 observation data due to their sparsity. Socio-hydrologic reanalysis can work as a reliable
523 and spatio-temporally homogeneous dataset and may be helpful to deepen the
524 understanding of human and water. In addition, socio-hydrologic reanalysis can be used
525 as initial condition to predict the future change of socio-hydrologic processes as
526 atmospheric scientists predict the future weather/climate using atmospheric reanalysis.
527 Since it is impossible to directly observe all state variables and parameters as initial
528 conditions, socio-hydrologic reanalysis is crucially important for accurate prediction.
529 Socio-hydrologic data assimilation has a high potential to improve the understanding of
530 the complex feedback between social and flood systems and predict their future. Our
531 idealized OSSE and real-data experiment reveal several important findings.

532

533 First, the sequential data assimilation can mitigate the negative impact of the uncertainty
534 in the input forcing on the simulation of socio-hydrologic state variables. We found that
535 the small perturbation of high water levels greatly affects the long-term trajectory of the
536 socio-hydrologic state variables as Viglione et al. (2014) found. It is necessary to
537 sequentially constrain the state variables and parameters by sequential data assimilation
538 if the input forcing is uncertain although previous studies on the model-data integration
539 in socio-hydrology mainly focused on parameter calibration assuming no uncertainty in
540 the input forcing (e.g., Barendrecht et al. 2019; Roobavannan et al. 2017; Ciullo et al.
541 2017; van Emmerik et al. 2014; Gonzales and Ajami 2017). To deeply understand the
542 socio-hydrologic processes, the long-term historical analysis should be performed.
543 Although there are many studies on the accurate reconstruction of the historical weather
544 condition (e.g., Toride et al. 2017), it may be necessary to tackle with the uncertainty in
545 hydrometeorological datasets used for the input forcing of the socio-hydrologic models.

546

547 Second, our SIRPF can efficiently improve the simulation of the socio-hydrologic state
548 variables using the sparsely distributed data. All model variables should not necessarily
549 be observed to constrain the model's state variables and parameters. In some cases,
550 observations of a single state variable are enough to reconstruct the accurate socio-

551 hydrologic state. In addition, observation intervals can be longer than 10-year. Since it is
552 difficult to obtain the large volume of data in socio-hydrology, this finding is promising.
553 We also give some insights about the informative observation types in the flood risk
554 model. With uncertain high water levels, observations of the intensity of flooding events
555 F and the height of levee H are not informative (i.e. the assimilation of these observations
556 cannot greatly improve the simulation skill) although the empirical data which can be
557 related to F and H may be easily found. On the other hand, observations of the size of the
558 human settlement G are informative to constrain the flood risk model. Model parameters
559 can be efficiently estimated by assimilating the state variables which is tightly related to
560 the targeted parameters, which is consistent to the findings of the idealized experiment by
561 Barendrecht et al. (2019).

562

563 Third, our SIRPF is robust to the imperfectness of the socio-hydrologic model. The
564 unknown parameters can be efficiently estimated by the sequential data assimilation.
565 While previous studies evaluated the trajectory in the whole study period to calibrate the
566 socio-hydrologic models by iteratively performing the long-term model integration (e.g.,
567 Barendrecht et al. 2019; Roobavannan et al. 2017; Ciullo et al. 2017; van Emmerik et al.
568 2014; Gonzales and Ajami 2017), we sequentially optimize parameters based on the

569 relatively short-term timeseries allowing parameters to temporally vary in the study
570 period. The advantage of this strategy is that we can deal with time-variant parameters as
571 previously demonstrated in the applications to hydrologic models (e.g., Pathiraja et al.
572 2018). In the model development, parameters are formulated as time-invariant values so
573 that the existence of time-variant parameters indicates the imperfect description of
574 dynamic models. Sequential data assimilation can mitigate the negative impact of this
575 imperfect model description. Vrugt et al. (2013) pointed out that the parameter
576 optimization by the sequential filters is unstable if parameter sensitivity temporally
577 changes (e.g., parameters affects the model's dynamics differently in the different
578 seasons), which may be the potential limitation of our strategy compared with Bayesian
579 inference based on the long-term trajectory such as Barendrecht et al. (2019).

580

581 The major limitation of this study is that we assume the modeled state variables can
582 directly be observed although it is difficult to directly observe state variables of the socio-
583 hydrologic models. For example, it is impossible to directly observe social awareness of
584 flood risk in the flood risk model and several previous studies obtained the proxy of the
585 social memory by interview data (Barendrecht et al. 2019) and the number of Google
586 searches (Gonzales and Ajami 2017). When these indirect observations are assimilated

587 into a model, the (non-linear) observation operator (see equation (9)), the assignment of
588 the observation error, and assimilation methods should be carefully designed as
589 previously discussed in the context of numerical weather prediction (e.g., Sawada et al.
590 2019; Okamoto et al. 2019; Minamide and Zhang 2017). Future work will focus on the
591 methodological development to efficiently assimilate observations in the social domain
592 with complicated structure of observation operators and errors.

593

594 **6. Conclusion**

595 In this study, we proposed to apply the sequential data assimilation to the socio-
596 hydrologic models. By several OSSEs and the real-data experiment in the flood risk
597 modeling, we found that our proposed SIRPF is robust to the imperfect input forcing and
598 the imperfect model. The sequential data assimilation is useful to reconstruct the socio-
599 hydrologic conditions from the inaccurate and sparsely distributed data and the imperfect
600 simulation.

601

602

603 **Acknowledgements**

604 We thank Di Baldassarre for sharing the original source code of the flood risk model. We
605 thank two anonymous referees for their constructive comments. Data Integration and
606 Analysis System (DIAS) provided us the computational resources.

607

608 **Code/Data availability**

609 Code and data are available upon the request to the corresponding author.

610

611 **Author Contribution**

612 YS designed the study. RH and YS jointly developed the data assimilation system for the
613 flood risk model and performed the numerical experiments. YS and RH contributed to
614 interpreting the results. YS wrote the first draft of the paper and RH contributed to editing
615 the paper.

616

617 **Competing interests**

618 The authors declare that they have no conflict of interest.

619

620 **References**

621 Barendrecht, M. H., Viglione, A., Kreibich, H., Merz, B., Vorogushyn, S., and Blöschl,
622 G.: The Value of Empirical Data for Estimating the Parameters of a
623 Sociohydrological Flood Risk Model. *Water Resources Research*.
624 <https://doi.org/10.1029/2018WR024128>, 2019

625 Bauer, P., Thorpe, A., and Brunet, G.: The quiet revolution of numerical weather
626 prediction. *Nature*, 525(7567), 47–55. <https://doi.org/10.1038/nature14956>, 2015

627 Ciullo, A., Viglione, A., Castellarin, A., Crisci, M., and Di Baldassarre, G.: Socio-
628 hydrological modelling of flood-risk dynamics: comparing the resilience of green
629 and technological systems. *Hydrological Sciences Journal*, 62(6), 880–891.
630 <https://doi.org/10.1080/02626667.2016.1273527>, 2017

631 Dang, Q., and Konar, M.: Trade Openness and Domestic Water Use. *Water Resources*
632 *Research*, 54(1), 4–18. <https://doi.org/10.1002/2017WR021102>, 2018

633 Di Baldassarre, G., Viglione, A., Carr, G., Kuil, L., Salinas, J. L., and Blöschl, G.: Socio-
634 hydrology: Conceptualising human-flood interactions. *Hydrology and Earth*
635 *System Sciences*, 17(8), 3295–3303. <https://doi.org/10.5194/hess-17-3295-2013>,
636 2013

637 Di Baldassarre, G., et al.: Socio-hydrology: Scientific Challenges in Addressing a Societal
638 Grand Challenge. *Water Resources Research*, 1–29.
639 <https://doi.org/10.1029/2018wr023901>, 2019

640 Gonzales, P., and Ajami, N.: Social and Structural Patterns of Drought-Related Water
641 Conservation and Rebound. *Water Resources Research*, 53(12), 10619–10634.
642 <https://doi.org/10.1002/2017WR021852>, 2017

643 Hersbach, H. et al.: Global reanalysis: goodbye ERA-Interim, hello ERA5, *ECMWF*
644 *Newsletter*, 159, 17-24, doi: [10.21957/vf291hehd7](https://doi.org/10.21957/vf291hehd7), 2019

645 Kobayashi, S., et al.: The JRA-55 Reanalysis: General Specifications and Basic
646 Characteristics. *Journal of the Meteorological Society of Japan*, 93, 5-48.
647 <https://doi.org/10.2151/jmsj.2015-001>, 2015

648 Kreibich, H., et al.: Adaptation to flood risk: Results of international paired flood event
649 studies. *Earth's Future*. <https://doi.org/10.1002/eff2.232>, 2017

650 Lievens, H., et al.: Joint Sentinel-1 and SMAP data assimilation to improve soil moisture
651 estimates. *Geophysical Research Letters*, 44(12), 6145–6153.
652 <https://doi.org/10.1002/2017GL073904>, 2017

653 Minamide, M., and Zhang, F: Adaptive Observation Error Inflation for Assimilating All-
654 Sky Satellite Radiance., *Monthly Weather Review*, 145, 1063–1081,
655 <https://doi.org/10.1175/MWR-D-16-0257.1>, 2017

656 Miyoshi, T., and Yamane, S.: Local Ensemble Transform Kalman Filtering with an
657 AGCM at a T159/L48 Resolution. *Monthly Weather Review*, 135(2002), 3841–
658 3861. <https://doi.org/10.1175/2007MWR1873.1>, 2007

659 Moradkhani, H., Hsu, K. L., Gupta, H., and Sorooshian, S.: Uncertainty assessment of
660 hydrologic model states and parameters: Sequential data assimilation using the
661 particle filter. *Water Resources Research*, 41(5), 1–17.
662 <https://doi.org/10.1029/2004WR003604>, 2005

663 Mostert, E.: An alternative approach for socio-hydrology: Case study research. *Hydrology
664 and Earth System Sciences*, 22(1), 317–329. [https://doi.org/10.5194/hess-22-317-
665 2018](https://doi.org/10.5194/hess-22-317-2018), 2018

666 Mount, N., J., et al.: Data-driven modelling approaches for sociohydrology: opportunities
667 and challenges within the Panta Rhei Science Plan. *Hydrological Sciences Journal*,
668 61(7), 1192-1208. <https://doi.org/10.1080/02626667.2016.1159683>, 2016

669 Okamoto, K, Sawada, Y, Kunii, M. Comparison of assimilating all-sky and clear-sky
670 infrared radiances from Himawari-8 in a mesoscale system. *Q J R Meteorol Soc.*,
671 *145*, 745-766. <https://doi.org/10.1002/qj.3463>, 2019

672 Pande, S., and Savenije, H. H. G.: A sociohydrological model for smallholder farmers in
673 Maharashtra, India. *Water Resources Research*, *52*(3), 1923–1947.
674 <https://doi.org/10.1002/2015WR017841>, 2016

675 Pathiraja, S., Anghileri, D., Burlando, P., Sharma, A., Marshall, L., and Moradkhani, H.:
676 Time-varying parameter models for catchments with land use change: the
677 importance of model structure, *Hydrol. Earth Syst. Sci.*, *22*, 2903–2919,
678 <https://doi.org/10.5194/hess-22-2903-2018>, 2018.

679 Penny, S. G., and Miyoshi, T.: *A local particle filter for high-dimensional geophysical*
680 *systems*. 391–405. <https://doi.org/10.5194/npg-23-391-2016>, 2016

681 Poterjoy, J., Wicker, L., and Buehner, M.: Progress toward the application of a localized
682 particle filter for numerical weather prediction. *Monthly Weather Review*, *147*(4),
683 1107–1126. <https://doi.org/10.1175/MWR-D-17-0344.1>, 2019

684 Qin, J., Liang, S., Yang, K., Kaihotsu, I., Liu, R., and Koike, T.: Simultaneous estimation
685 of both soil moisture and model parameters using particle filtering method through

686 the assimilation of microwave signal. *Journal of Geophysical Research*, 114(D15),
687 1–13. <https://doi.org/10.1029/2008JD011358>, 2009

688 Rasmussen, J., Madsen, H., Jensen, K. H., and Refsgaard, J. C.: Data assimilation in
689 integrated hydrological modeling using ensemble Kalman filtering: evaluating the
690 effect of ensemble size and localization on filter performance. *Hydrology and Earth
691 System Sciences*, 19(7), 2999–3013. <https://doi.org/10.5194/hess-19-2999-2015>,
692 2015

693 Roobavannan, M., Kandasamy, J., Pande, S., Vigneswaran, S., and Sivapalan, M.: Role
694 of Sectoral Transformation in the Evolution of Water Management Norms in
695 Agricultural Catchments: A Sociohydrologic Modeling Analysis. *Water Resources
696 Research*, 53(10), 8344–8365. <https://doi.org/10.1002/2017WR020671>, 2017

697 Sawada, Y., Koike, T., and Walker, J. P.: A land data assimilation system for simultaneous
698 simulation of soil moisture and vegetation dynamics. *J. Geophys. Res. Atmos.*, 120,
699 5910– 5930. doi: [10.1002/2014JD022895](https://doi.org/10.1002/2014JD022895), 2015

700 Sawada, Y., Nakaegawa, T. and Miyoshi, T.: Hydrometeorology as an inversion problem:
701 Can river discharge observations improve the atmosphere by ensemble data
702 assimilation? *Journal of Geophysical Research: Atmospheres*, 123, 848– 860.
703 <https://doi.org/10.1002/2017JD027531>, 2018

704 Sawada, Y., Okamoto, K., Kunii, M., and Miyoshi, T.: Assimilating every-10-minute
705 Himawari-8 infrared radiances to improve convective predictability. *Journal of*
706 *Geophysical Research: Atmospheres*, 124, 2546–2561.
707 <https://doi.org/10.1029/2018JD029643>, 2019

708 Sivapalan, M., Savenije, H.H.G. and Blöschl, G.: Socio-hydrology: A new science of
709 people and water. *Hydrol. Process.*, 26: 1270-1276. doi:[10.1002/hyp.8426](https://doi.org/10.1002/hyp.8426), 2012

710 Sivapalan, M., Konar, M., Srinivasan, V., Chhatre, A., Wutich, A., Scott, C. A., and
711 Wescoat, J. L.: Socio-hydrology: Use-inspired water sustainability science for the
712 Anthropocene, *Earth's Future*, 2, 225–230. <https://doi.org/10.1002/2013EF000164>,
713 2014.

714 Toride, K., Neluwala, P., Kim, H. and Yoshimura, K.: Feasibility Study of the
715 Reconstruction of Historical Weather with Data Assimilation. *Mon. Wea. Rev.*, **145**,
716 3563–3580, <https://doi.org/10.1175/MWR-D-16-0288.1>, 2017

717 Van Emmerik, T. H. M., et al.: Socio-hydrologic modeling to understand and mediate the
718 competition for water between agriculture development and environmental health:
719 Murrumbidgee River basin, Australia. *Hydrology and Earth System Sciences*,
720 18(10), 4239–4259. <https://doi.org/10.5194/hess-18-4239-2014>, 2014

721 Viglione, A., et al.: Insights from socio-hydrology modelling on dealing with flood risk -
722 Roles of collective memory, risk-taking attitude and trust. *Journal of Hydrology*,
723 518(PA), 71–82. <https://doi.org/10.1016/j.jhydrol.2014.01.018>, 2014

724 Vrugt, J. A., ter Braak, C. J. F., Diks, C. G. H., and Schoups, G.: Hydrologic data
725 assimilation using particle Markov chain Monte Carlo simulation: Theory, concepts
726 and applications. *Advances in Water Resources*, 51, 457–478.
727 <https://doi.org/10.1016/j.advwatres.2012.04.002>, 2013

728 Yu, D. J., Sangwan, N., Sung, K., Chen, X., and Merwade, V.: Incorporating institutions
729 and collective action into a sociohydrological model of flood resilience. *Water*
730 *Resources Research*, 53(2), 1336–1353. <https://doi.org/10.1002/2016WR019746>,
731 2017

732

733

734

735

736 **Table 1.** Parameters of the flood risk model

737

| | description | Values | Ranges in data assimilation | ω in equation (17) |
|-----------------|---|--------|--------------------------------|------------------------------|
| ξ_H | proportion of additional high water level due to levee heightening | 0.5 | - | - |
| α_H | parameter related to the slope of the floodplain and the resilience of the human settlement | 0.01 | - | - |
| ρ_E | maximum relative growth rate | 0.02 | - | - |
| λ_E | critical distance from the river beyond which the settlement can no longer grow | 5000 | - | - |
| γ_E | Cost of levee raising | 0.5 | 0.2-5.0 | 0.01 |
| λ_P | distance at which people would accept to live when they remember past floods whose total consequences were perceived as a total destruction of the settlement | 12000 | - | |
| φ_P | rate by which new properties can be built | 10000 | 1000-50000 | 100 |
| ε_T | safety factor for levees rising | 1.1 | - | - |
| κ_T | rate of decay of levees | 0.001 | 0-0.0015 | 0.0000025 |
| α_S | proportion of shock after flooding if levees are risen | 0.5 | - | - |
| μ_S | memory loss rate | 0.05 | 0-0.4 | 0.0025 |

738

739

740 **Table 2.** RMSE of the no data assimilation experiment (NoDA) and the data
 741 assimilation experiment (DA) in which all observations are assimilated every 10 years
 742 with 5000 ensembles in the experiment 1 (see section 3.1).

743

| | NoDA | DA |
|---|-----------------------|-----------------------|
| G | 1.06×10^6 | 1.64×10^4 |
| D | 3.60×10^2 | 3.92×10^1 |
| H | 2.65 | 1.41 |
| M | 1.08×10^{-1} | 8.32×10^{-2} |

744

745

746 **Table 3.** RMSE of the no data assimilation experiment (NoDA) and the data
 747 assimilation experiment (DA) in which all observations are assimilated every 10 years
 748 with 5000 ensembles in the experiment 2 (see section 3.2).
 749

| | NoDA | DA |
|-------------|-----------------------|-----------------------|
| G | 2.97×10^6 | 1.64×10^4 |
| D | 1.86×10^3 | 1.01×10^2 |
| H | 9.35 | 1.63 |
| M | 2.24×10^{-1} | 8.99×10^{-2} |
| γ_E | 2.08 | 4.27×10^{-1} |
| φ_P | 1.72×10^4 | 3.81×10^3 |
| κ_T | 4.12×10^{-4} | 2.36×10^{-4} |
| μ_S | 1.55×10^{-1} | 2.43×10^{-2} |

750

751

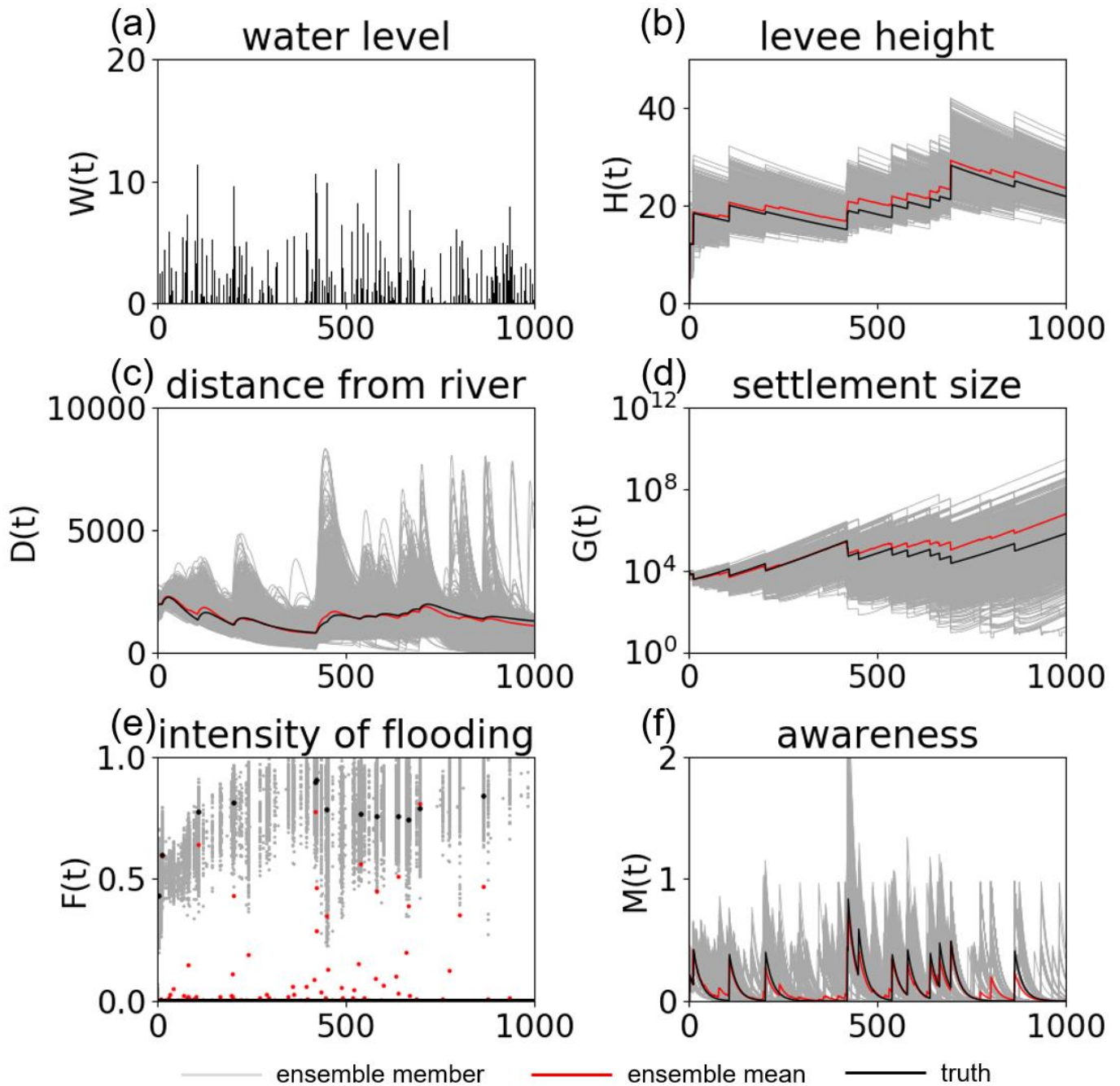
752 **Table 4.** RMSE of the no data assimilation experiment (NoDA) and the data
 753 assimilation experiment (DA) in which all observations are assimilated every 10 years
 754 with 5000 ensembles in the experiment 3 (see section 3.3).

755

| | NoDA | DA |
|-------------|-----------------------|-----------------------|
| G | 2.91×10^6 | 6.20×10^3 |
| D | 2.20×10^3 | 2.02×10^2 |
| H | 9.21 | 1.65 |
| M | 2.48×10^{-1} | 1.05×10^{-1} |
| γ_E | 2.08 | 5.20×10^{-1} |
| φ_P | 1.98×10^4 | 7.68×10^3 |
| κ_T | 4.12×10^{-4} | 2.54×10^{-4} |
| μ_S | 1.60×10^{-1} | 3.03×10^{-2} |

756

757

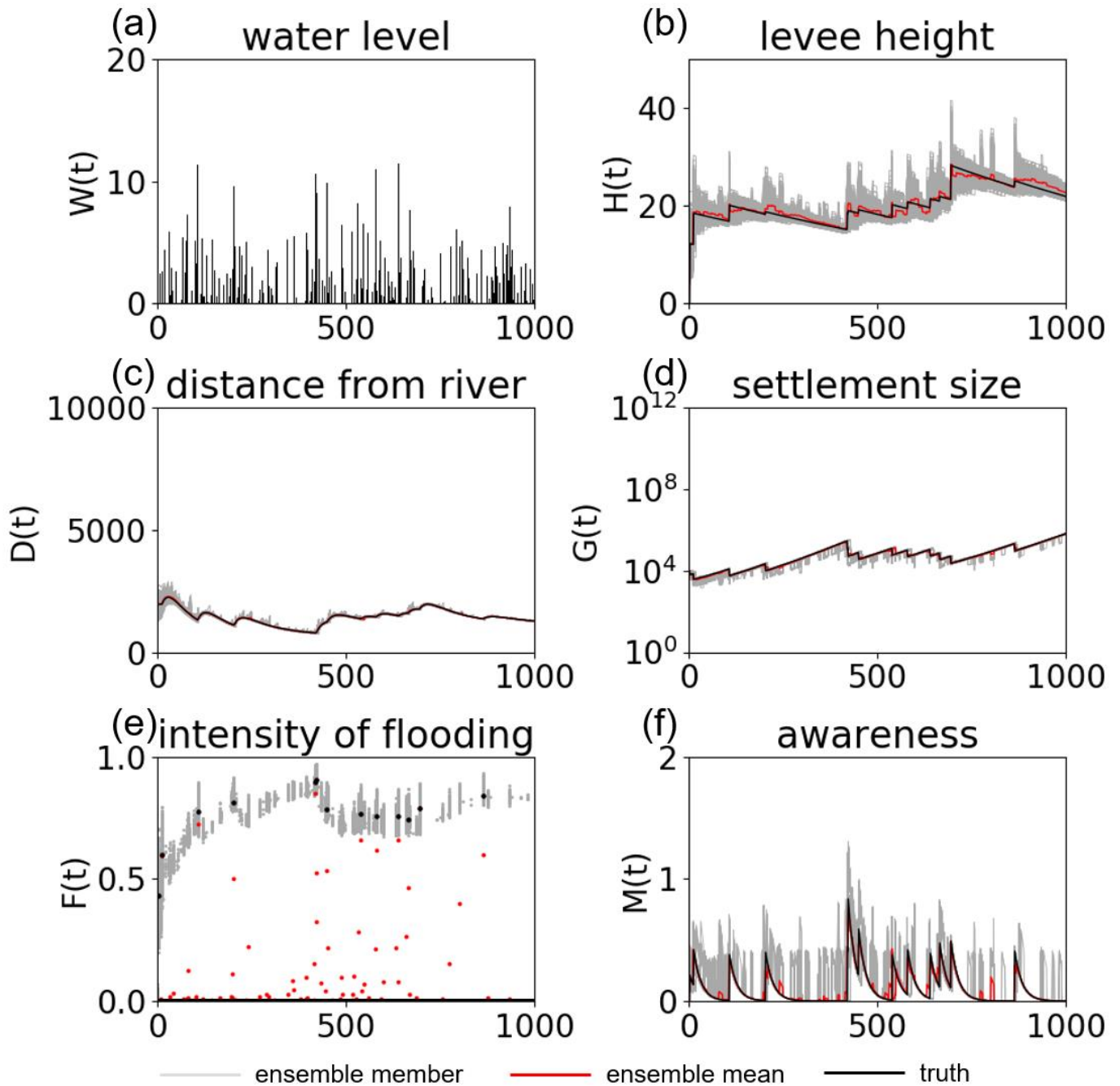


758

759 **Figure 1.** Timeseries of (a) high water level $W(t)$, (b) the flood protection level (or levee height) $H(t)$, (c) the
 760 distance of the center of mass of the human settlement from the river $D(t)$, (d) the size of the human settlement
 761 $G(t)$, (e) the intensity of flooding events $F(t)$, and (f) the social awareness of the flood risk $M(t)$ simulated by
 762 5000 ensembles with uncertain high water levels and no data assimilation in the experiment 1 (see section

763 3.1.1). The time step is annual. Grey, red, and black lines are the ensemble members, their mean, and the
764 synthetic truth, respectively.

765



766

767

768

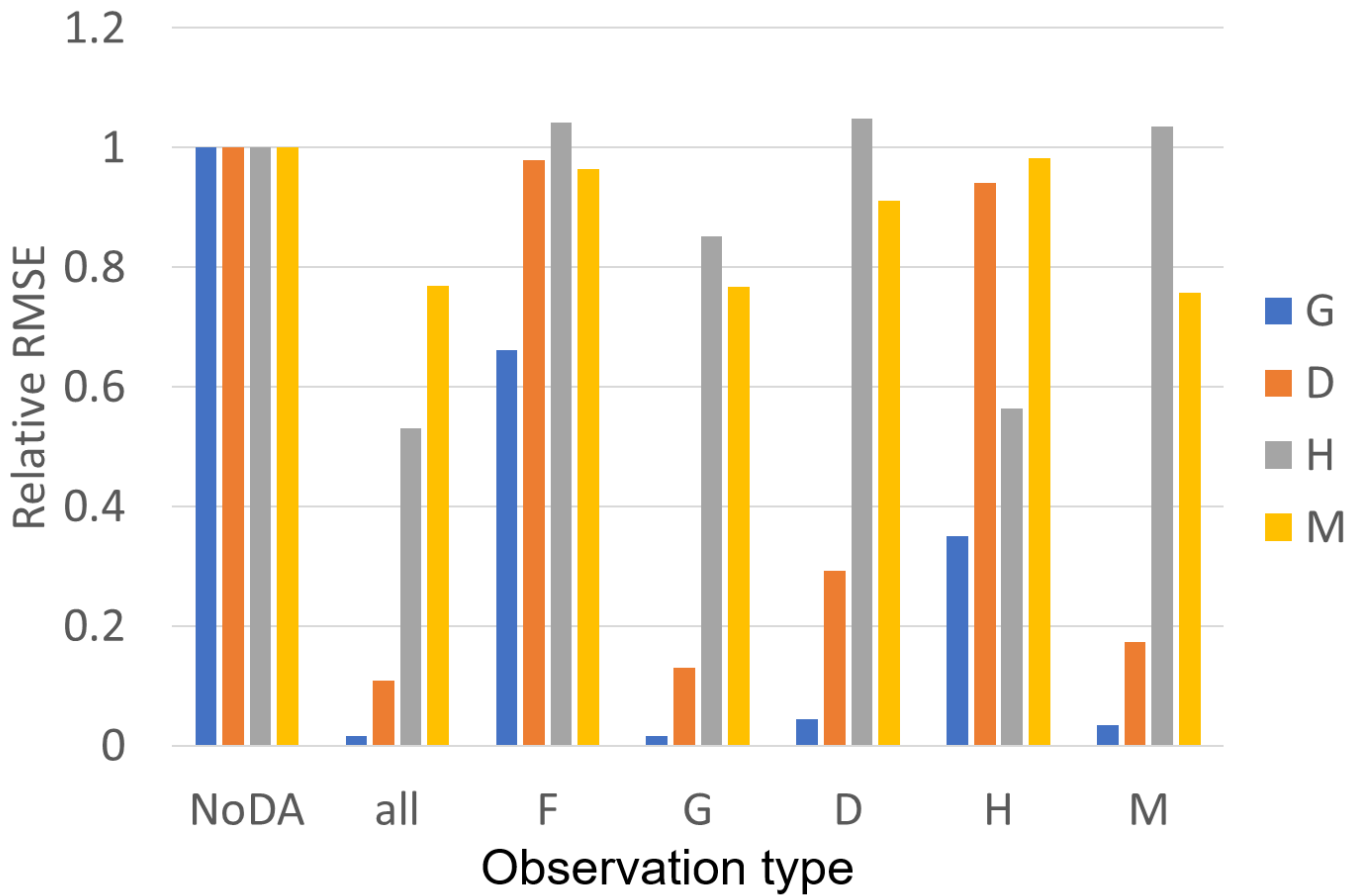
769

770

Figure 2. Timeseries of (a) high water level $W(t)$, (b) the flood protection level (or levee height) $H(t)$, (c) the distance of the center of mass of the human settlement from the river $D(t)$, (d) the size of the human settlement $G(t)$, (e) the intensity of flooding events $F(t)$, and (f) the social awareness of the flood risk $M(t)$ simulated by the data assimilation experiment in which the observations of F , G , D , H , and M are assimilated into the model

771 every 10 years with 5000 ensembles in the experiment 1 (see section 3.1.1). The time step is annual. Grey, red,
772 and black lines are the ensemble members, their mean, and the synthetic truth, respectively.

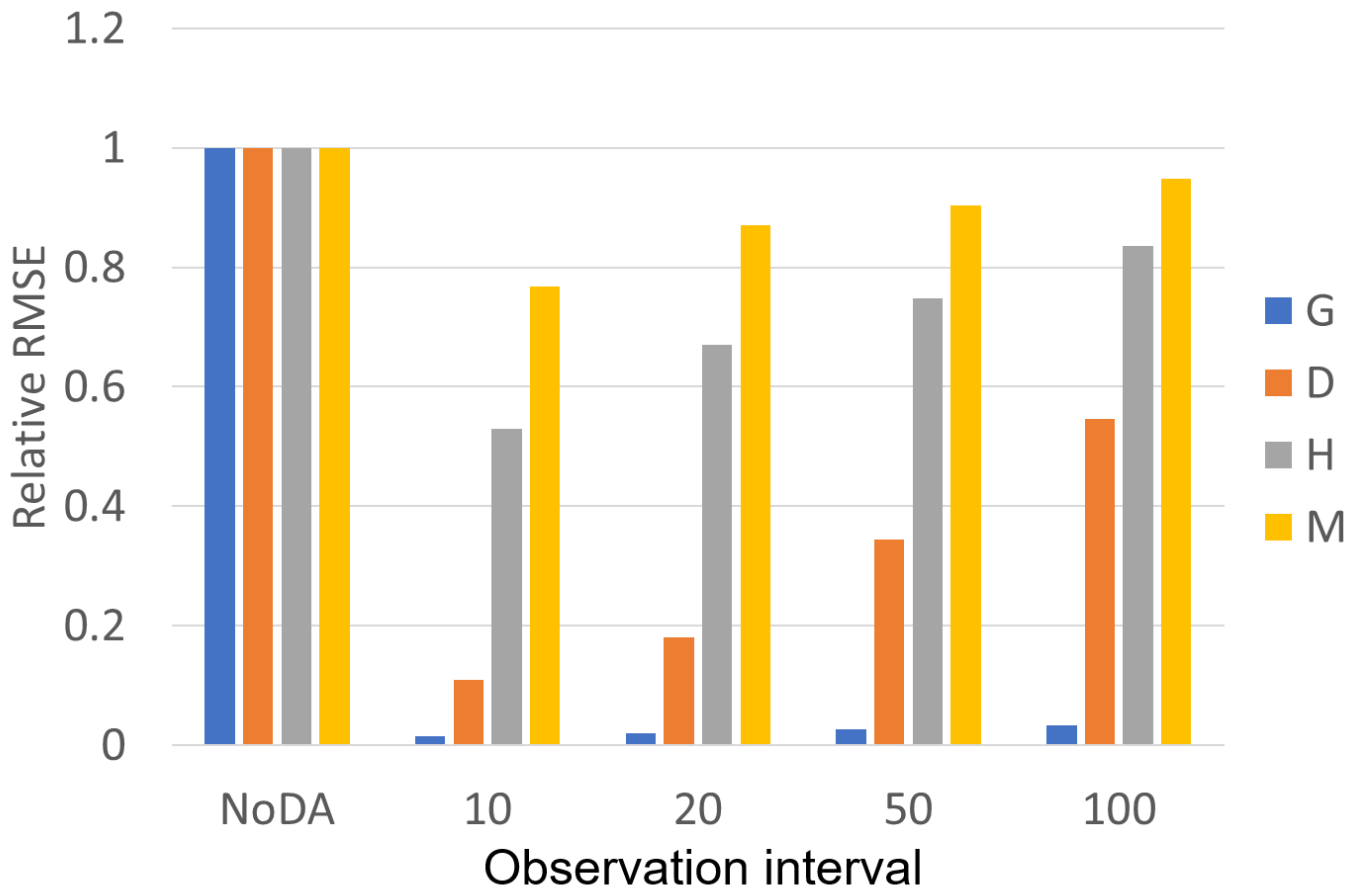
773



774

775 **Figure 3.** The ratio of RMSEs of the no data assimilation experiment (NoDA) to those of the data assimilation
 776 experiments in which all of observations (F, G, D, H, and M) are assimilated (all) and each one of them is
 777 assimilated in the experiment 1 (see section 3.1.1). Blue, orange, gray, and yellow bars are RMSEs of the size
 778 of the human settlement $G(t)$, the center of mass of the human settlement from the river $D(t)$, the flood
 779 protection level (or levee height) $H(t)$, and the social awareness of the flood risk $M(t)$.

780



781

782

Figure 4. The ratio of RMSEs of the no data assimilation experiment (NoDA) to those of the data assimilation

783

experiments in which all of observations (F, G, D, H, and M) are assimilated every 10, 20, 50, and 100 years

784

in the experiment 1 (see section 3.1.1). Blue, orange, gray, and yellow bars are RMSEs of the size of the

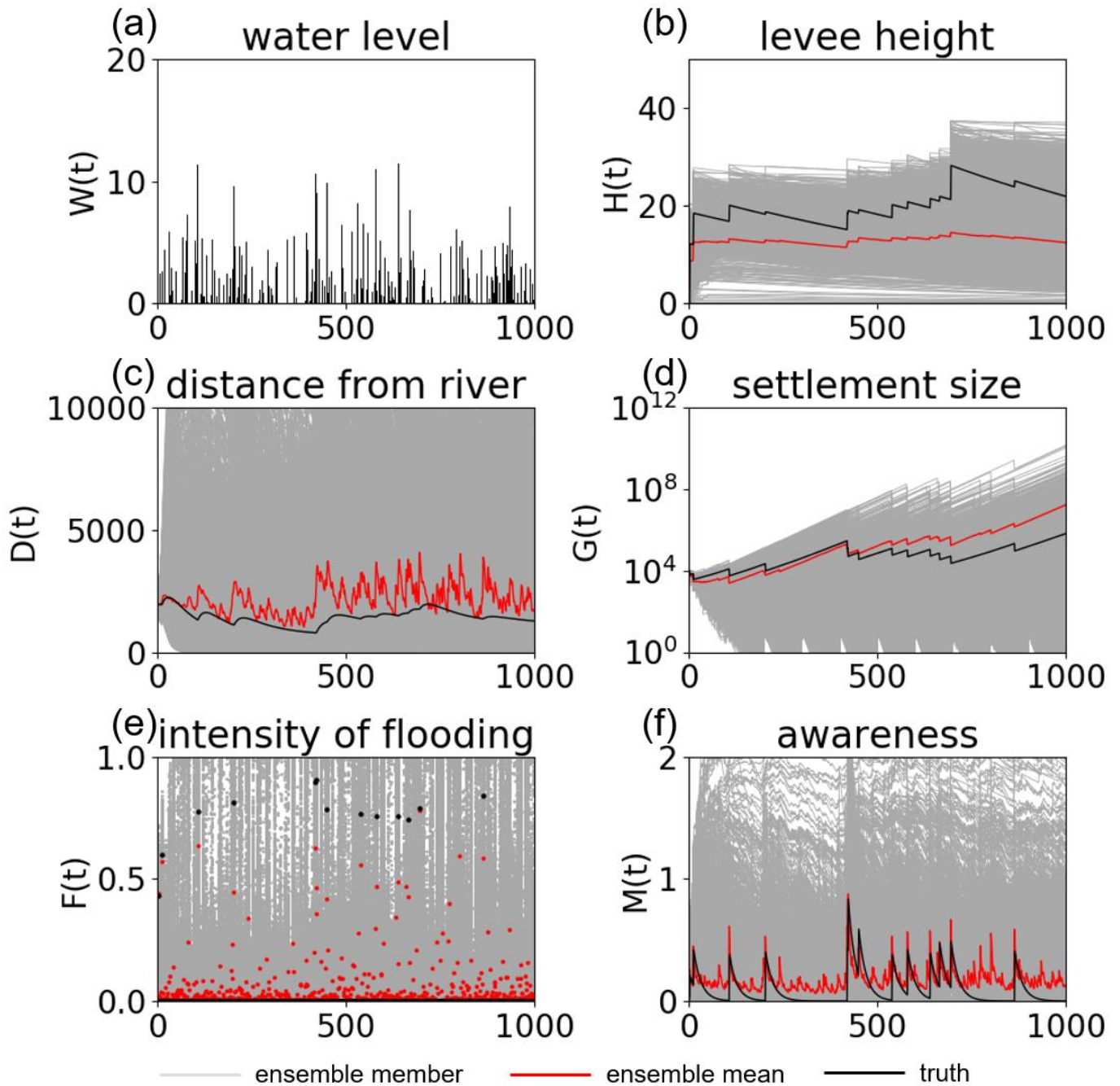
785

human settlement $G(t)$, the center of mass of the human settlement from the river $D(t)$, the flood protection

786

level (or levee height) $H(t)$, and the social awareness of the flood risk $M(t)$.

787

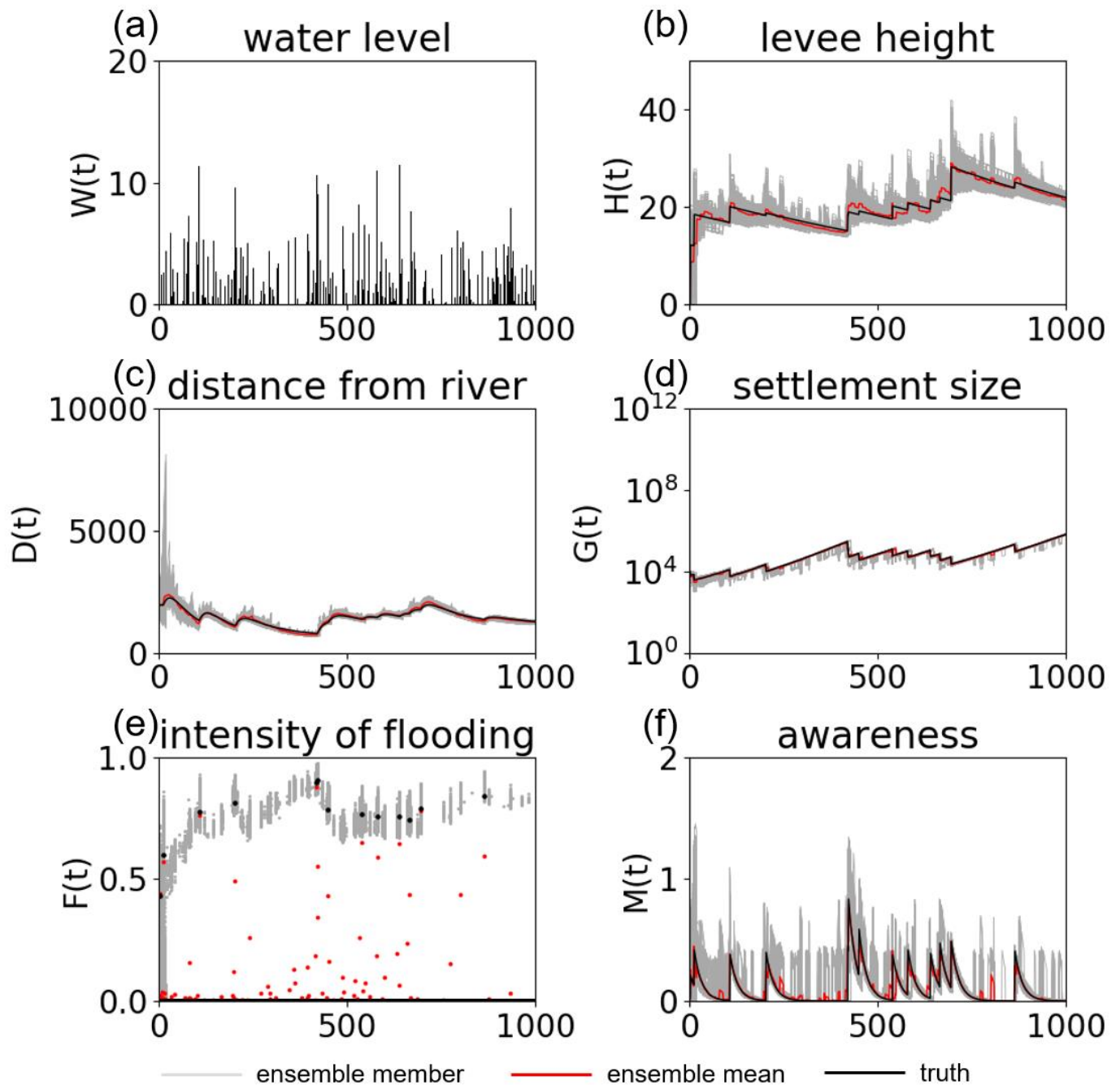


788

789 **Figure 5.** Timeseries of (a) high water level $W(t)$, (b) the flood protection level (or levee height) $H(t)$, (c) the
 790 distance of the center of mass of the human settlement from the river $D(t)$, (d) the size of the human settlement
 791 $G(t)$, (e) the intensity of flooding events $F(t)$, and (f) the social awareness of the flood risk $M(t)$ simulated by
 792 5000 ensembles with uncertain high water levels and no data assimilation in the experiment 2 (see section

793 3.1.2). The time step is annual. Grey, red, and black lines are the ensemble members, their mean, and the
794 synthetic truth, respectively.

795



797

798

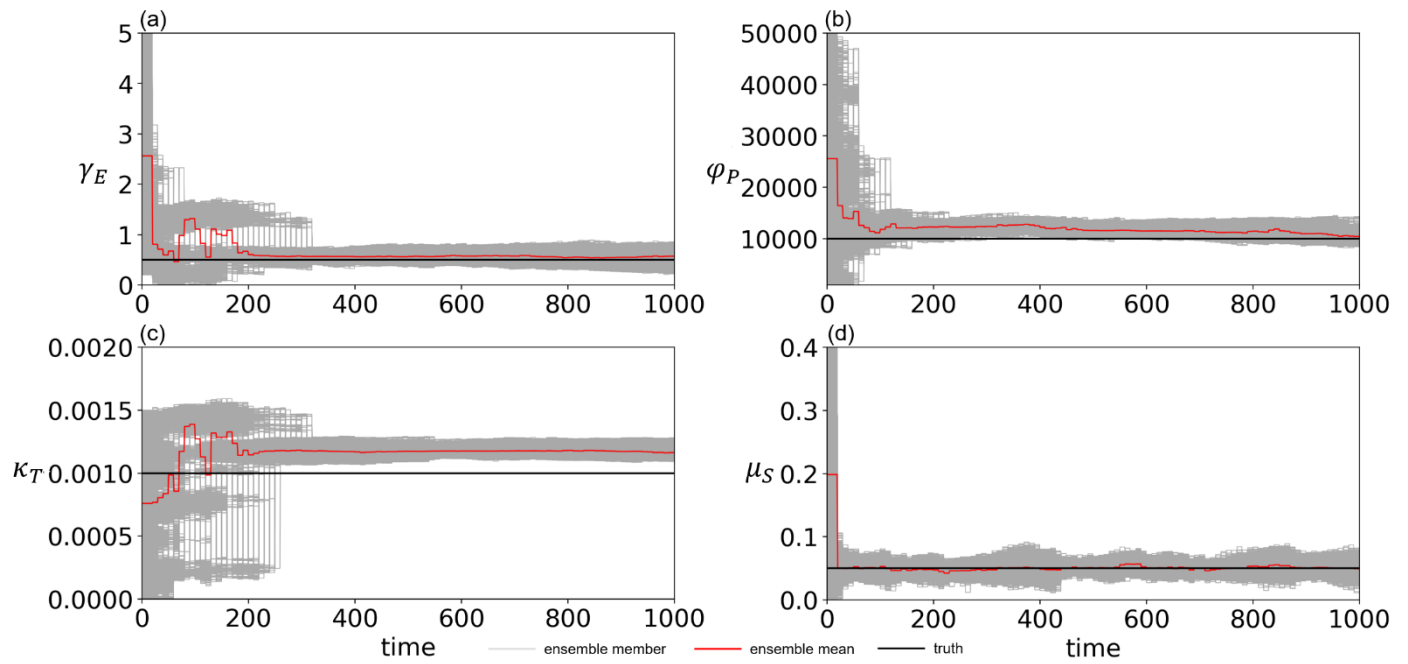
799

800

801

Figure 6. Timeseries of (a) high water level $W(t)$, (b) the flood protection level (or levee height) $H(t)$, (c) the distance of the center of mass of the human settlement from the river $D(t)$, (d) the size of the human settlement $G(t)$, (e) the intensity of flooding events $F(t)$, and (f) the social awareness of the flood risk $M(t)$ simulated by the data assimilation experiment in which the observations of F , G , D , H , and M are assimilated into the model

802 every 10 years with 5000 ensembles in the experiment 2 (see section 3.1.2). The time step is annual. Grey, red,
803 and black lines are the ensemble members, their mean, and the synthetic truth, respectively.



804

805

806

807

808

809

810

Figure 7. Timeseries of (a) the cost of levee raising γ_E , (b) the rate by which new properties can be built φ_P , (c) the rate of decay of levees κ_T , (d) memory loss rate μ_S estimated by the data assimilation of all observations (F, G, D, H, and M) with 5000 ensembles every 10 years in the experiment 2 (see section 3.1.2). The time step is annual. Grey, red, and black lines are the ensemble members, their mean, and the synthetic truth, respectively.

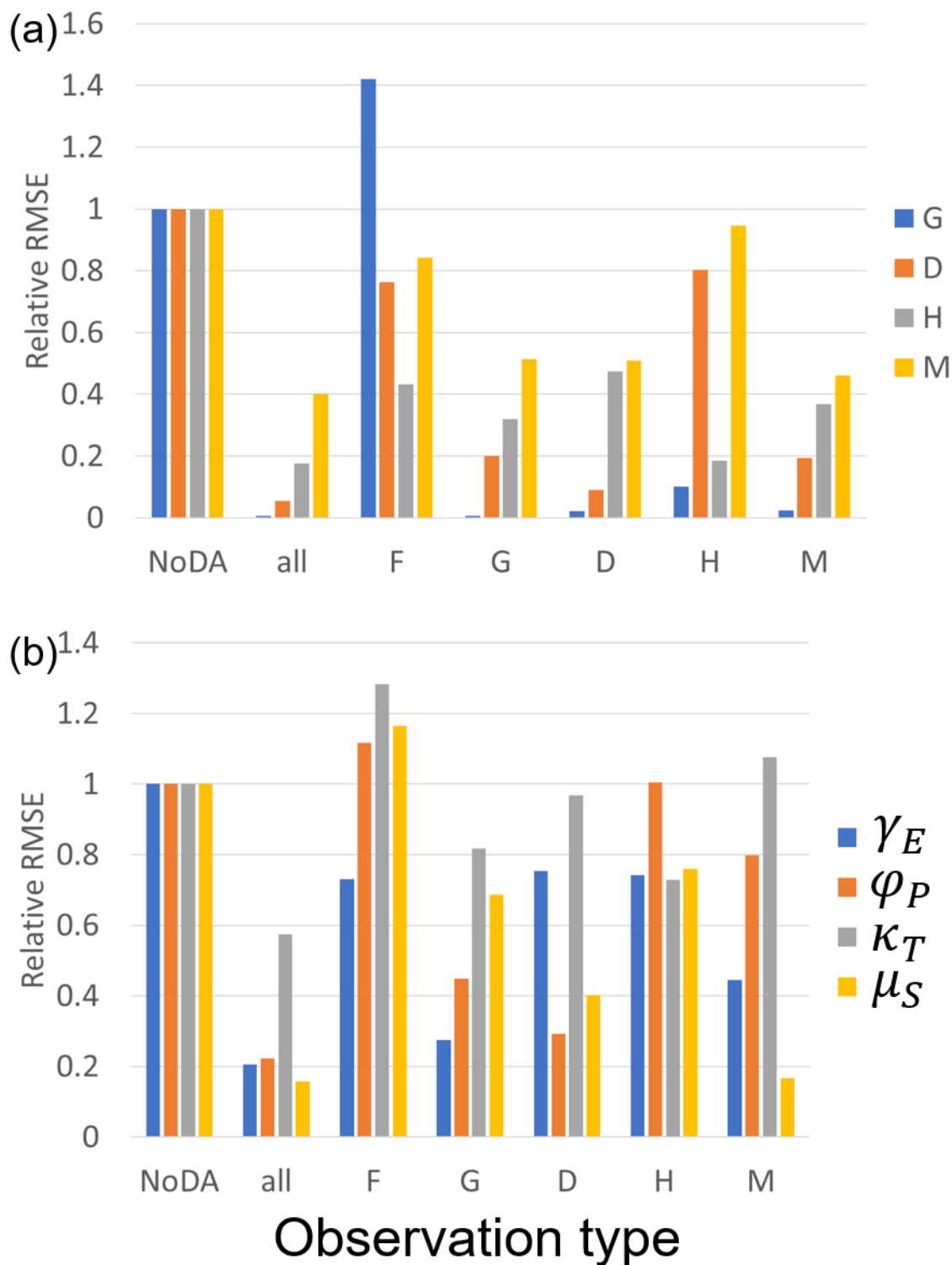
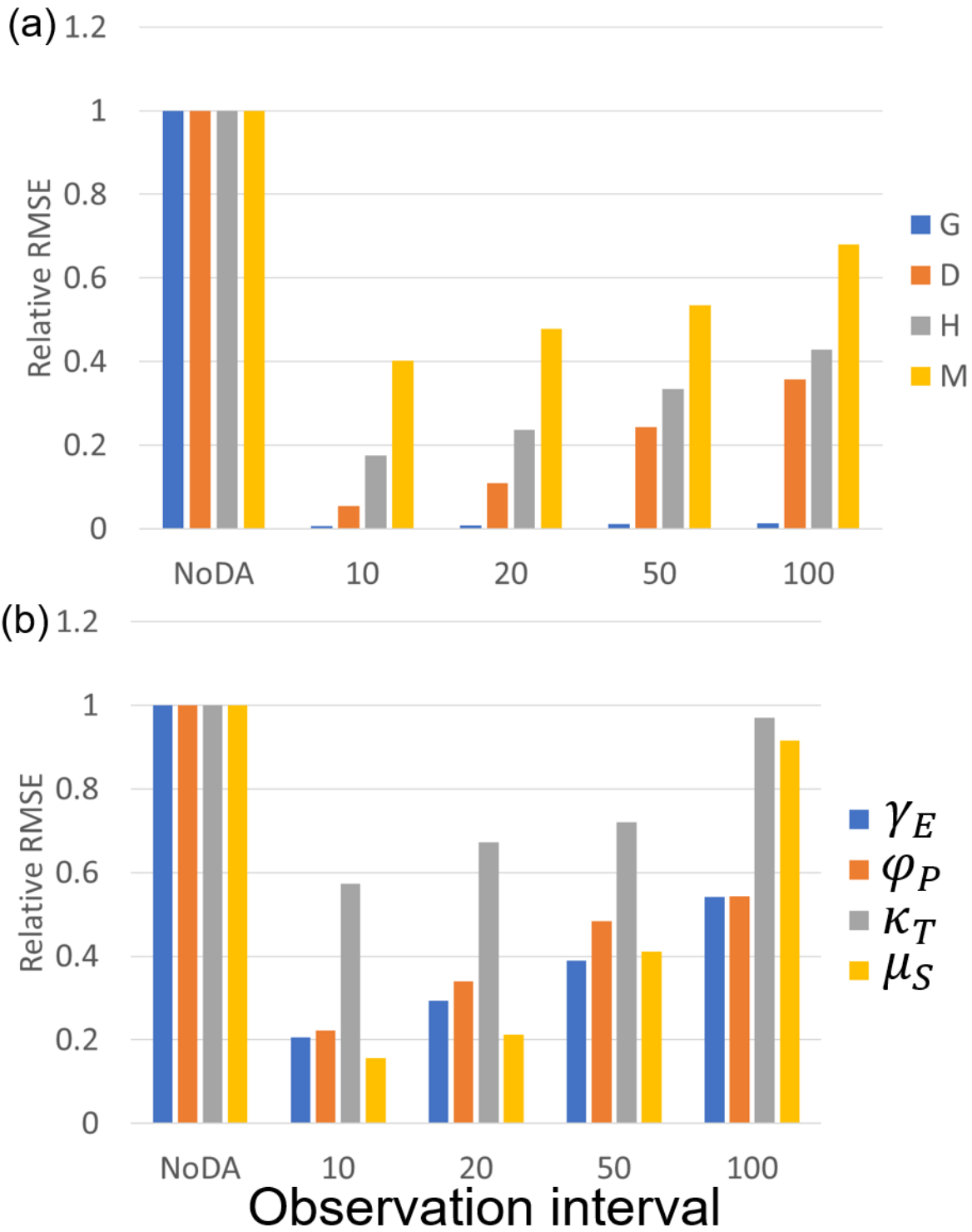


Figure 8. The ratio of RMSEs of the no data assimilation experiment (NoDA) to those of the data assimilation experiments in which all of observations (F, G, D, H, and M) are assimilated (all) and each one of them is assimilated in the experiment 2 (see section 3.1.2). (a) Blue, orange, gray, and yellow bars are RMSEs of the

816 size of the human settlement $G(t)$, the center of mass of the human settlement from the river $D(t)$, the flood
817 protection level (or levee height) $H(t)$, and the social awareness of the flood risk $M(t)$. (b) Blue, orange, gray,
818 and yellow bars are RMSEs of the cost of levee raising γ_E , the rate by which new properties can be built φ_P ,
819 the rate of decay of levees κ_T , memory loss rate μ_S .

820

821



822

823

824

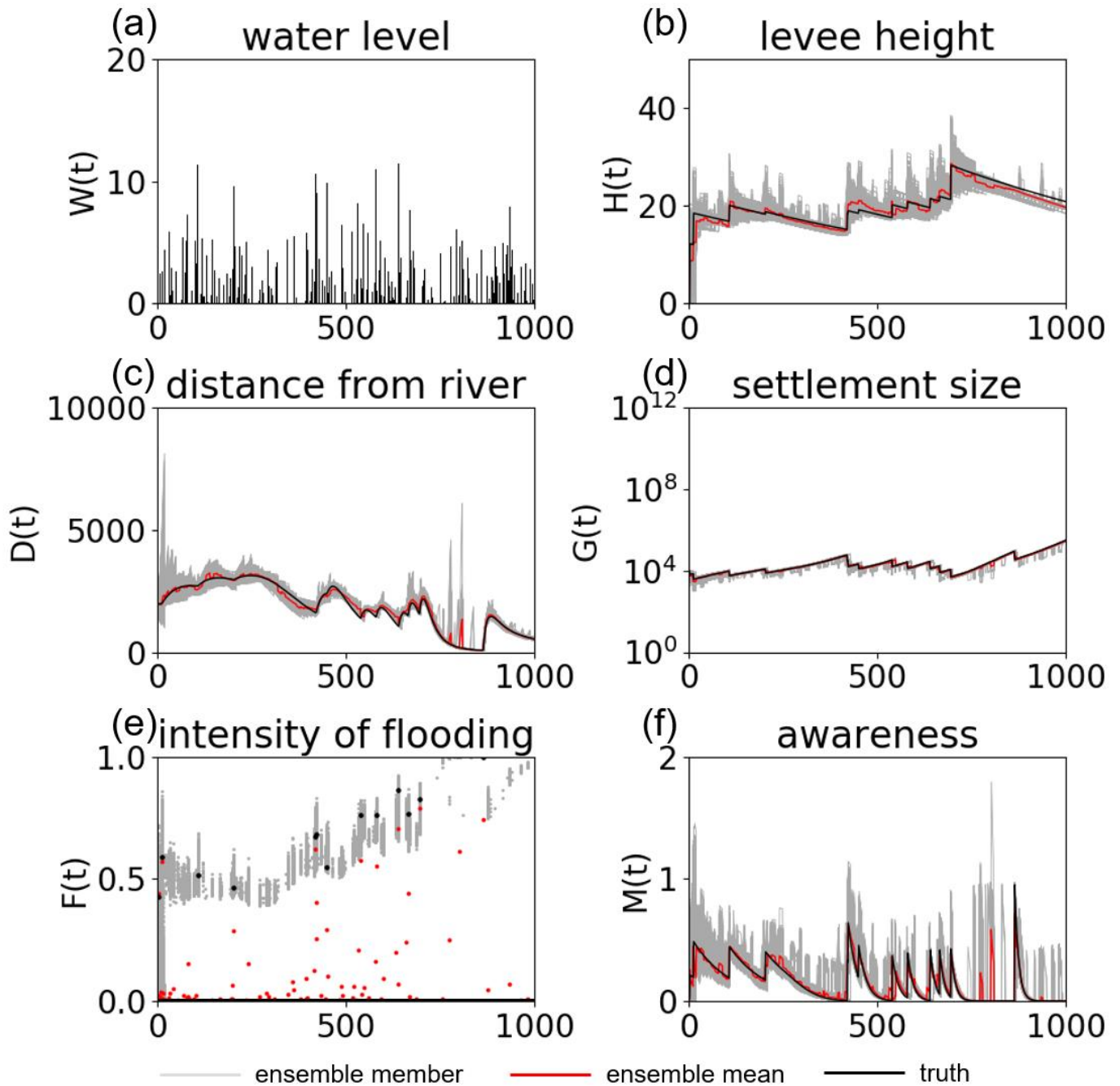
825

Figure 9. The ratio of RMSEs of the no data assimilation experiment (NoDA) to those of the data assimilation experiments in which all of observations (F, G, D, H, and M) are assimilated every 10, 20, 50, and 100 years in the experiment 2 (see section 3.1.2). (a) Blue, orange, gray, and yellow bars are RMSEs of the size of the

826 human settlement $G(t)$, the center of mass of the human settlement from the river $D(t)$, the flood protection
827 level (or levee height) $H(t)$, and the social awareness of the flood risk $M(t)$. (b) Blue, orange, gray, and yellow
828 bars are RMSEs of the cost of levee raising γ_E , the rate by which new properties can be built φ_P , the rate of
829 decay of levees κ_T , memory loss rate μ_S .

830

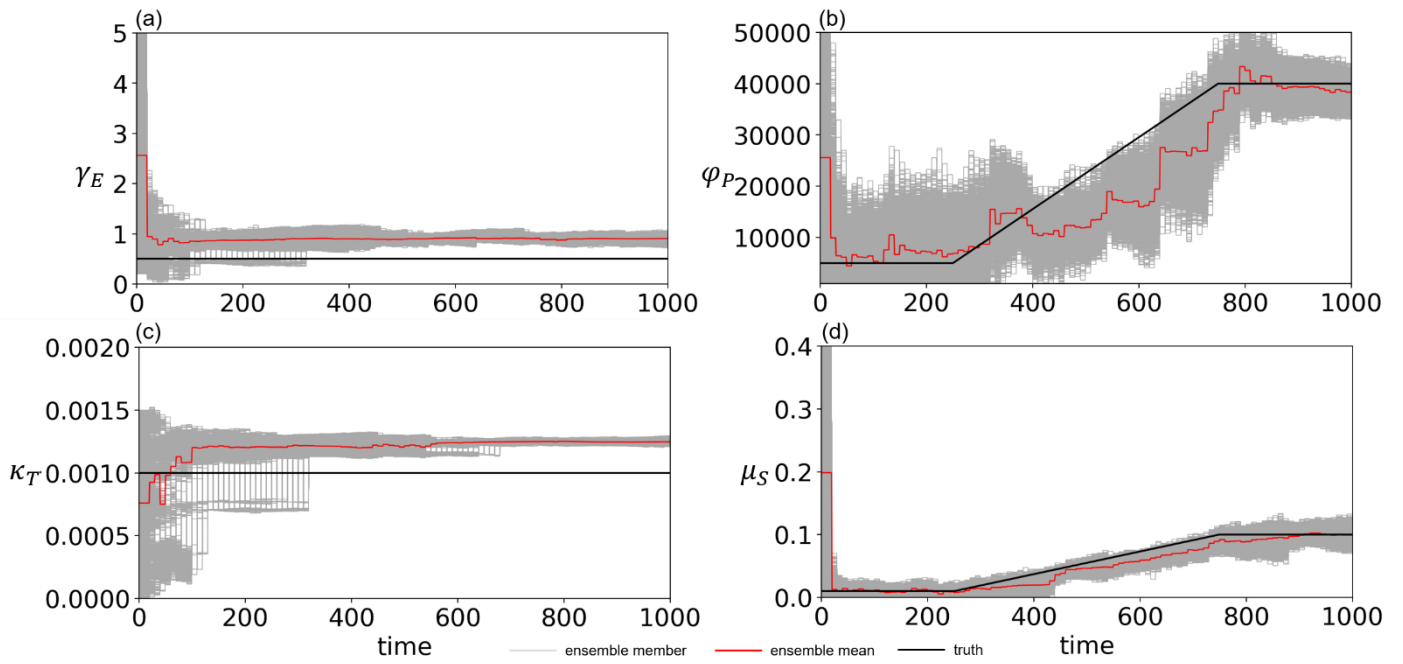
831



832

833 **Figure 10.** Timeseries of (a) high water level $W(t)$, (b) the flood protection level (or levee height) $H(t)$, (c) the
 834 distance of the center of mass of the human settlement from the river $D(t)$, (d) the size of the human settlement
 835 $G(t)$, (e) the intensity of flooding events $F(t)$, and (f) the social awareness of the flood risk $M(t)$ simulated by
 836 the data assimilation experiment in which the observations of F , G , D , H , and M are assimilated into the model

837 every 10 years with 5000 ensembles in the experiment 3 (see section 3.1.3). The time step is annual. Grey, red,
838 and black lines are the ensemble members, their mean, and the synthetic truth, respectively.



839

840

841

842

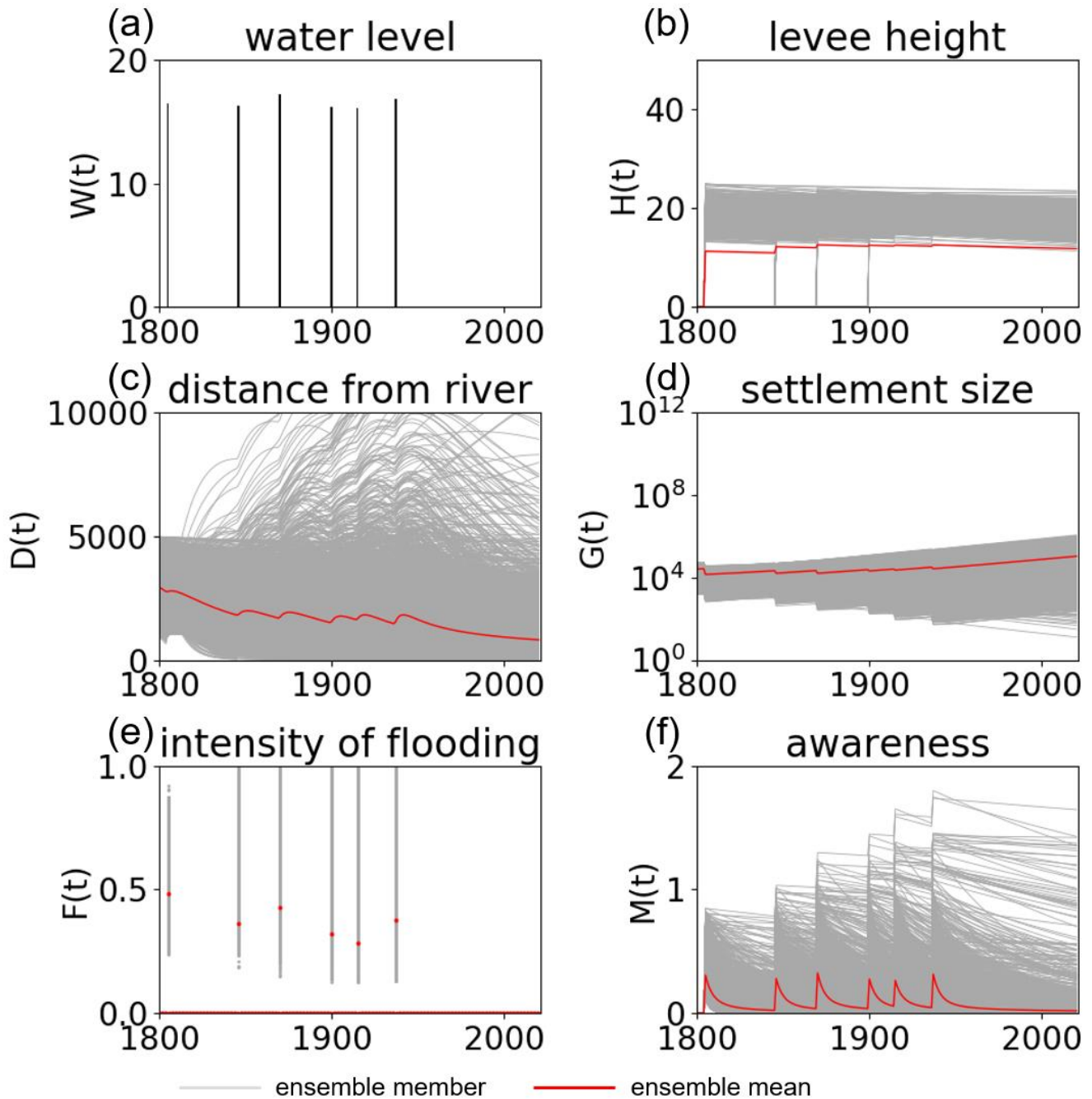
843

844

845

846

Figure 11. Timeseries of (a) the cost of levee raising γ_E , (b) the rate by which new properties can be built φ_P , (c) the rate of decay of levees κ_T , (d) memory loss rate μ_S estimated by the data assimilation of all observations (F, G, D, H, and M) with 5000 ensembles every 10 years in the experiment 3 (see section 3.1.3). The time step is annual. Grey, red, and black lines are the ensemble members, their mean, and the synthetic truth, respectively.

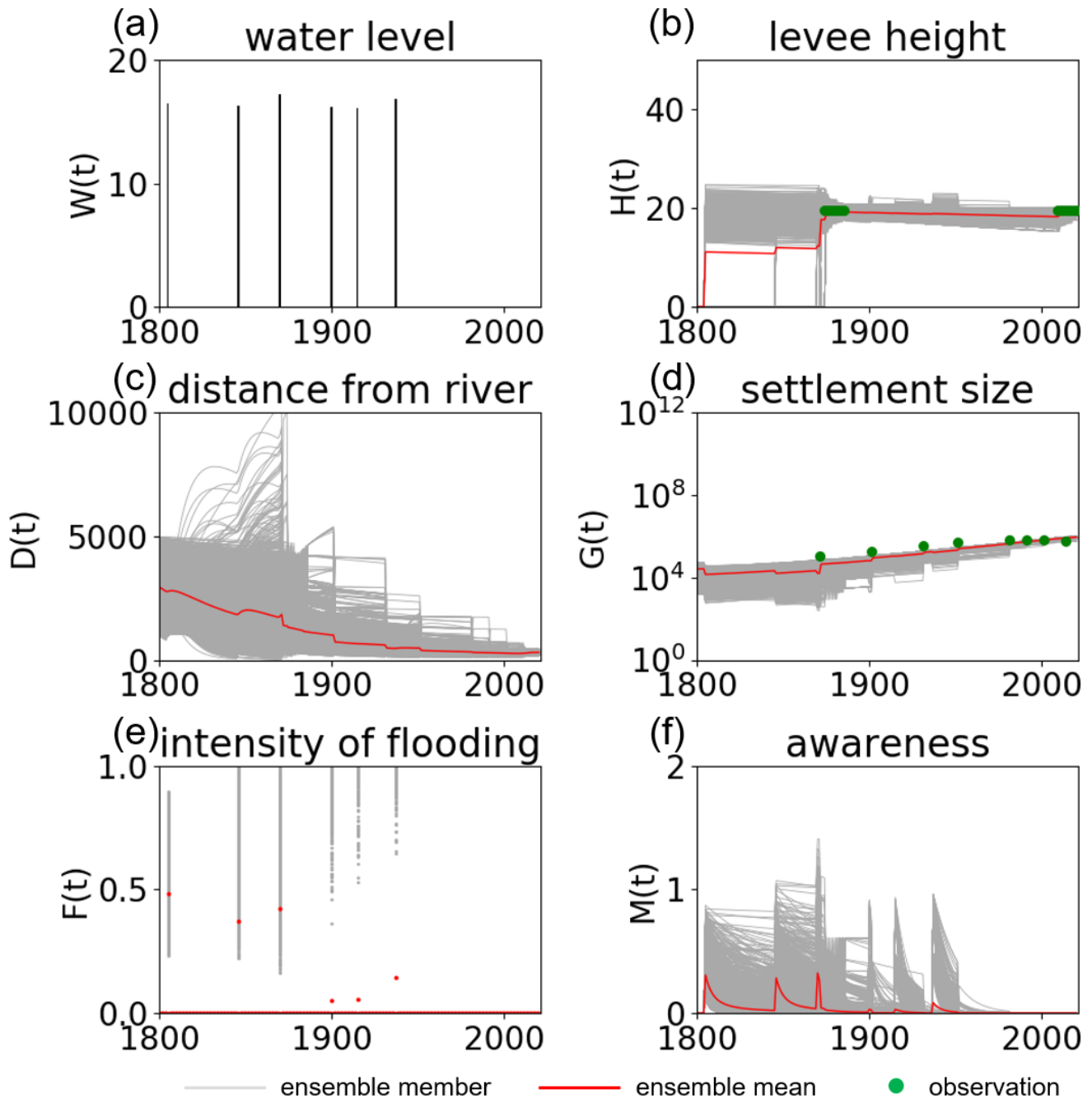


847

848 **Figure 12.** Timeseries of (a) high water level $W(t)$, (b) the flood protection level (or levee height) $H(t)$, (c) the
 849 distance of the center of mass of the human settlement from the river $D(t)$, (d) the size of the human settlement
 850 $G(t)$, (e) the intensity of flooding events $F(t)$, and (f) the social awareness of the flood risk $M(t)$ simulated by
 851 5000 ensembles with uncertain high water levels and no data assimilation in the real-world experiment in the

852 city of Rome. The time step is annual. Grey, and red lines are the ensemble members and their mean,
853 respectively.

854



855

856

857

858

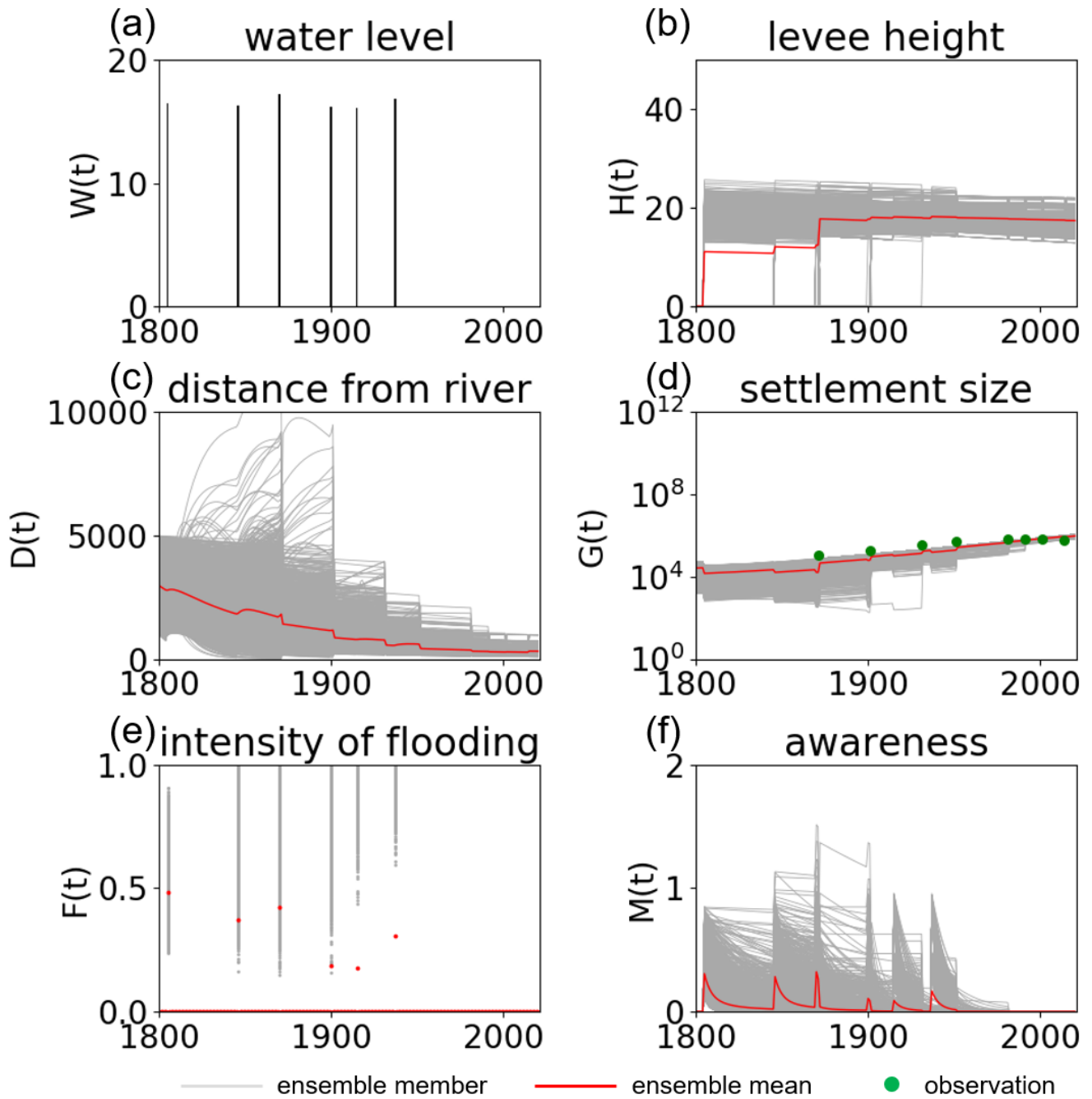
859

Figure 13. Timeseries of (a) high water level $W(t)$, (b) the flood protection level (or levee height) $H(t)$, (c) the distance of the center of mass of the human settlement from the river $D(t)$, (d) the size of the human settlement $G(t)$, (e) the intensity of flooding events $F(t)$, and (f) the social awareness of the flood risk $M(t)$ simulated by the data assimilation experiment in which the real-world observations of G and H (green dots) are assimilated

860 into the model with 5000 ensembles in the real-world experiment in the city of Rome. The time step is annual.

861 Grey, and red lines are the ensemble members and their mean, respectively.

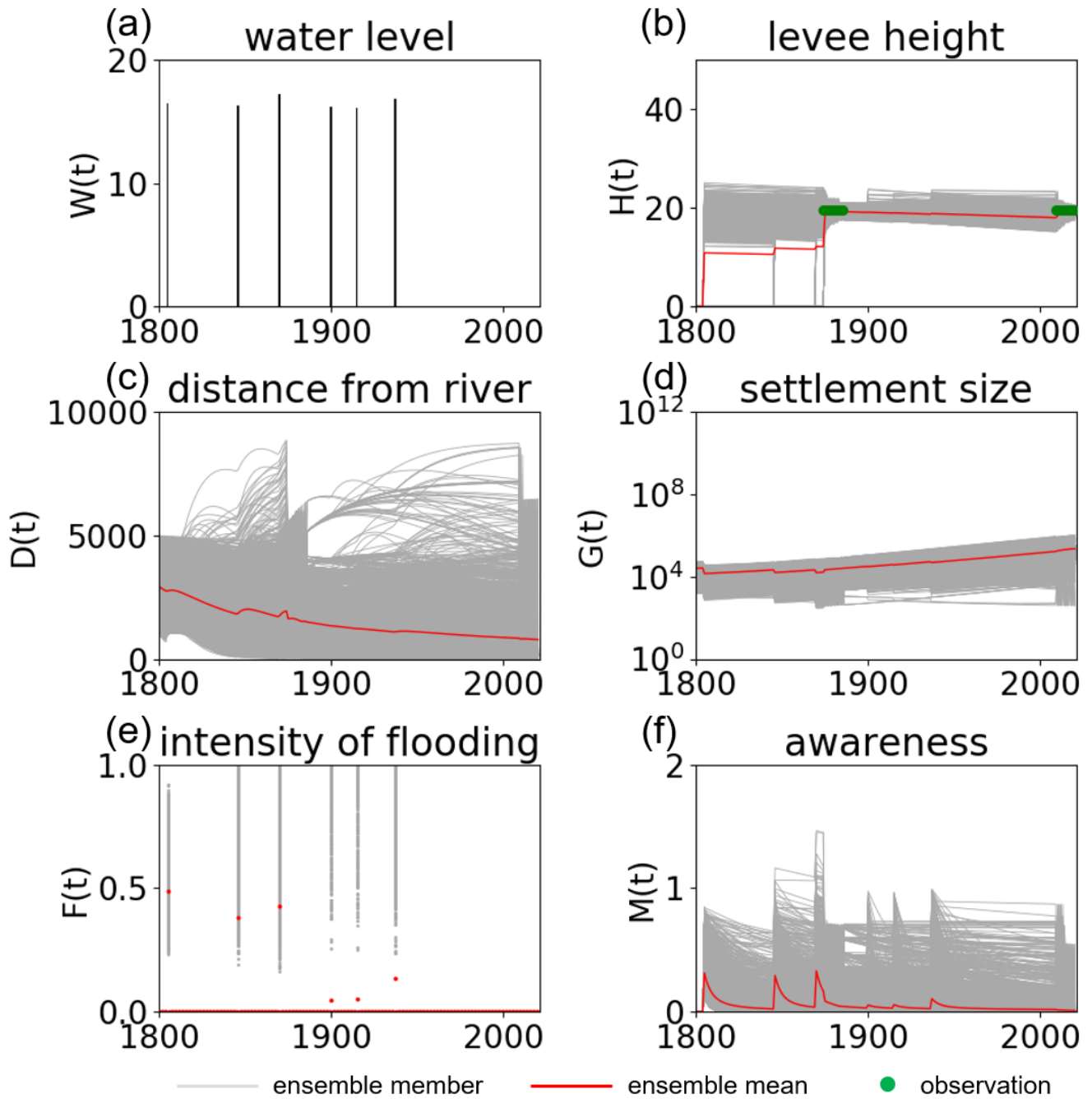
862



863

864 **Figure 14.** Same as Figure 13 but only real data of G are assimilated.

865



866

867 **Figure 15.** Same as Figure 13 but only real data of H are assimilated.

868